ION TRANSPORT MODELING FOR RETINAL ROD PHOTORECEPTOR CELLS

A Thesis presented to
the Faculty of the Graduate School
at the University of Missouri

In Partial Fulfillment of the Requirements for the Degree
Master of Science

---

by
XIAOZHEN WANG

Dr. Jinglu Tan, Thesis Supervisor

JULY 2010

The undersigned, appointed by the Dean of the Graduate School, have examined the thesis entitled

ION TRANSPORT MODELING
FOR RETINAL ROD PHOTORECEPTOR CELLS

Presented by Xiaozhen Wang

A candidate for the degree of Master of Science

And hereby certify that, in their opinion, it is worthy of acceptance.

_____
Jinglu Tan, Ph.D., Department of Biological Engineering

_____
Kristina Narfström, Ph.D., Department of Veterinary Medicine & Surgery

_____
Kevin Gillis, Ph.D., Department of Biological Engineering

ACKNOWLEDGEMENTS

I would like to give thanks to my supervisor, Dr. Jinglu Tan, who has been advising and supporting me throughout this work.

I would like to express thanks to my committee members, Dr. Kristina Narfström and Dr. Kevin Gillis, for their guidance and encouragement during my Master's program. Thanks are extended to Dr. Jinhua Yu, Dr. Ya Guo and Mr. Sri Waluyo.

I owe a special thanks to my whole family that have been encouraging and supporting me all the time.

TABLE OF CONTENTS

LIST OF FIGURES

Figure Page

LIST OF TABLES

Table Page

ION TRANSPORT MODELING

FOR RETINAL ROD PHOTORECEPTOR CELLS

Xiaozhen Wang

Dr. Jinglu Tan, Thesis Supervisor

ABSTRACT

In this study, a mathematical model is developed to describe the ion transport activities associated with the response of rod photoreceptor to light stimulus. In the model, the cell body is modeled as two capacitors connected via the connecting cilium. Roles of different ion channels during a photoreceptor light response are analyzed, and the relations between changes in ion concentration and response currents are assessed. Methods are developed for computing the membrane potential from ion concentrations and relating the material and electrical resistances. The steady state under different conditions can be uniquely defined with only three measured values.

The model can effectively describe the rod photoreceptor response to different light stimuli. Model simulation of the a-wave for progressive narrowing of the connecting cilium corresponds well with published literature on hereditary retinal degeneration of Abyssinian cats. Reductions in amplitude and changes in the a-wave waveform are observed in different stages of the disease. Changes in the receptor response amplitude may not be measurable till the conductance of the connecting cilium is reduced to a comparable magnitude of the ion channels. The model can provide quantitative information of ionic activities, changes in ion concentrations and membrane voltage in

the outer segment and the inner compartment. The ionic envirronment is found to be different between the outer segment and the inner compartment. During receptor response, changes in the outer segment appear to be stronger and quicker than those in the inner compartment. Reductions in the connecting cilium transport can reset the dark resting state.

CHAPTER 1

INTRODUCTION

The visual system is very important and complex. Our visual experience is initiated in the retina. When light enters the eye, it travels through the cornea and hits the back of the eye where the retina lies. The light is then converted into an electrical signal that propagates through the optic nerve to the brain. The cells that are responsible for transducing light are the photoreceptors, which are among the best understood sensory cells.

For years the retina has been a research field that bears extensive studies. Instead of being a peripheral sensory organ, it is part of the central nervous system; yet it has a relatively simple structure compared to other brain regions. Only six major classes of neurons compose the neuronal structure of the retina. The synaptic organization is complex but anatomical arrangement is in an orderly fashion with the neurons positioned in different layers in the retina. For these reasons, the retina serves as an important model for understanding the processing of signals within complex neural circuits of brain regions.

Many methods have been used in order to understand retina function. The electroretinogram (ERG) has been frequently used, both in research and in clinical diagnosis of diseases (Hood and Birch, 1990; Narfstrom and Ekesten, 1998; Katz et al., 2005; Vaegan and Narfstrom, 2008; Jeong et al., 2009). It is an electrical recording of the light-induced response from the retina *in vivo*, containing signals produced by different retina cells.

Functional degenerations resulting from aging or diseases can be inferred from changes in ERG.

The initial part of ERG recording, the ERG a-wave, is considered as solely a response of photoreceptors located at the first layer of the retina. The rod photoreceptors can sense light and give electrical responses through a transient suppression of its circulating current. The response is a result of opening and closing of different ion channels located in cell membranes, and will cause a series of changes in the concentrations of different ion species, which, in return, will have an effect on the response itself (Molday and Kaupp, 2000).

Extensive studies at the molecular level have advanced the understanding of the underlying mechanisms of the phototransduction process within photoreceptor cells. This has made it possible to develop models based on the actual biophysical processes.

Analytical approaches and modeling have been applied to analyze the a-wave; however, most existing models are empirical fittings with little connection to the molecular mechanisms. There has not been a reported model construct to simulate the light response based on the ionic activities in a rod photoreceptor.

The objective of this study was to anlyze the roles of different ion channels in shaping a photoreceptor response, and the relationship between transport through the connecting cilium and the response current by developing a mathematical model for vertebrate rod photoreceptor cells. Specifically, three ion species: K^+, Na^+, and Ca^{2+}, and five types of ion channels in the rod photoreceptor were considered in this study. Experiment data from

bright-flash analysis on Abyssinian cats with hereditary retinal degeneration were used to validate the model.

The thesis is divided into five chapters. The first chapter states the motivation and objectives of this study. The second chapter reviews the literature that provides the background for model construction and analysis. A mathematical model developed in this study is presented in Chapter 3, which accounts for the ionic activities within the rod photoreceptor cell and describes the electric response of rod photoreceptors to light. Chapter 4 presents the simulation results from the proposed model. The model predictions are compared with experiment data and discussed. Finally in Chapter 5, conclusions of the study are drawn with recommendations for future work.

CHAPTER 2

LITERATURE REVIEW

The retina lies at the back of the eye and is roughly 0.5mm thick. It can sense and convert light into electric signals that are transmitted to the brain through the optic nerve. There are generally six major classes of neurons layered inside the retina: photoreceptor cell, horizontal cell, bipolar cell, amacrine cell, Müller cell and ganglion cell y(Cajal 1972; Snodderly et al., 1984).

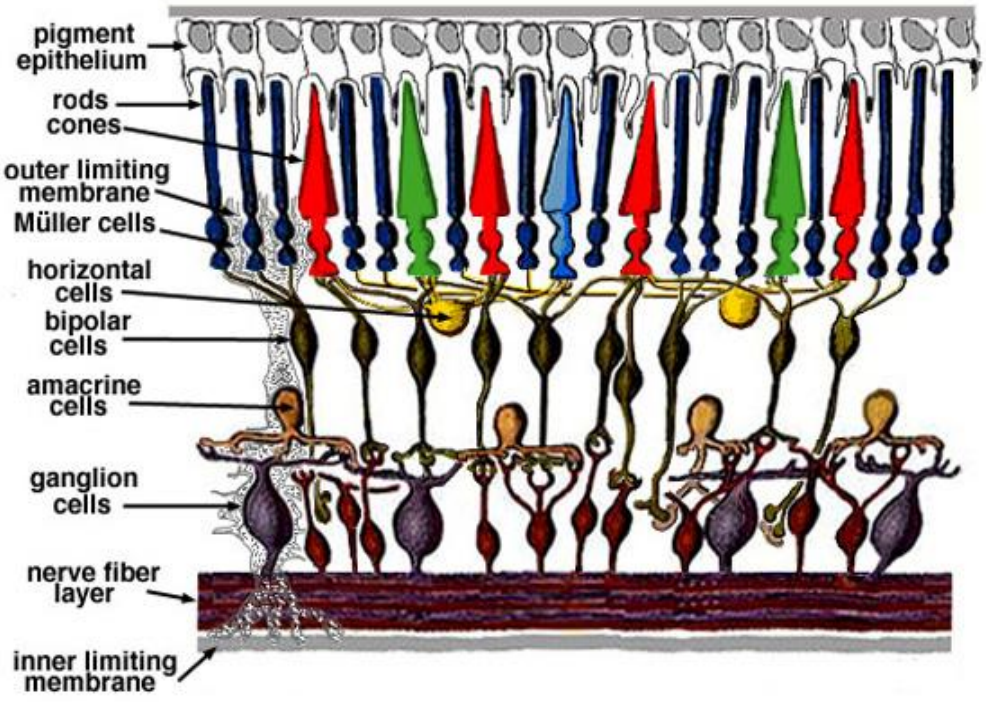

Figure 2.1 Simple diagram of the organization of the retina.
http://webvision.med.utah.edu/sretina.html

The photoreceptor cells lie in the outer retina. They provide the mechanism that converts light into electric signals.

The bipolar cells and horizontal cells are in the inner nuclear layer. They receive input from the photoreceptor cells. According to the function, horizontal cells can be divided into two classes. One type can sense the amount of light that strikes the photoreceptors, while the other type generates responses according to the color of light stimuli. The bipolar cells are also divided into two groups: the 'ON' and 'OFF' bipolar cells, according to how the cell responds to low-intensity light spotted at the center of the receptive field.

The amacrine cells have an axonless body, and support the lateral interconnections in the inner plexiform layer. They have been identified to have a lot of anatomical classes.

For the retina, the output neurons are the ganglion cells, which project to the lateral geniculate nucleus in the thalamus. Their specific functions are yet to be further explored.

2.1 Photoreceptor Cells in the Retina: Rods and Cones

2.1.1 Structure

The photoreceptor cells of the retina are light-sensitive. They absorb light and convert it into electric signals that propagate to their synaptic terminals, where neurotransmitter glutamate is released to reach second-order neurons of horizontal cells and bipolar cells. Eventually the information is signaled to the brain.

Photoreceptor cells are considered to be of two major classes: the rod photoreceptors, and the cone photoreceptors. Figure 2.2 shows a scanning electron micrograph of the rods and cones of the primate retina, in which rods are pictured as the slim rod-shaped structure filling the area between the larger cones at the bottom. In the mammalian retina, one type of rod photoreceptors and three types of cone photoreceptors are present. The rod photoreceptors have drawn attention during the last few years for their involvement in several human hereditary diseases, such as the human retinitis pigmentosa (RP) (Narfstrom, 1985b; Ehinger et al., 1991).

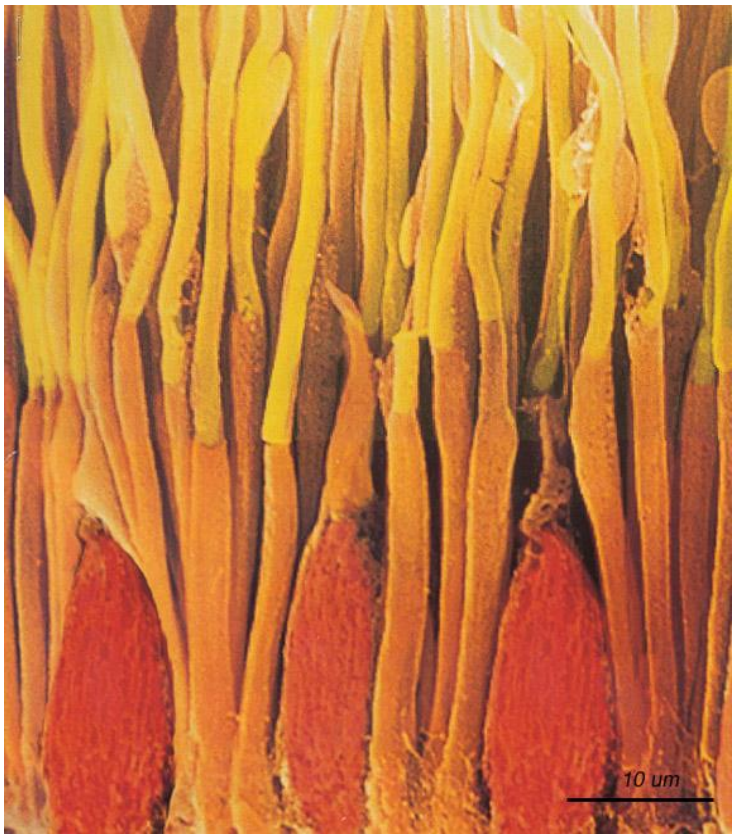

Figure 2.2. Scanning electron micrograph of the rods and cones of the primate retina. Image adapted from one by Ralph C. Eagle/Photo Researchers, Inc.

The rods and cones are polarized cells that have similar structures, as illustrated in Figure 2.3. It can be observed that the photoreceptor is divided into an outer segment region and inner segment region which connects to the synaptic terminal. The rod outer segment region contains folded membrane discs with opsin that is critical to phototransduction. The inner segment hosts structures such as mitochondria, nucleus, and endoplasmic reticulum that provides energy and synthesizes proteins.

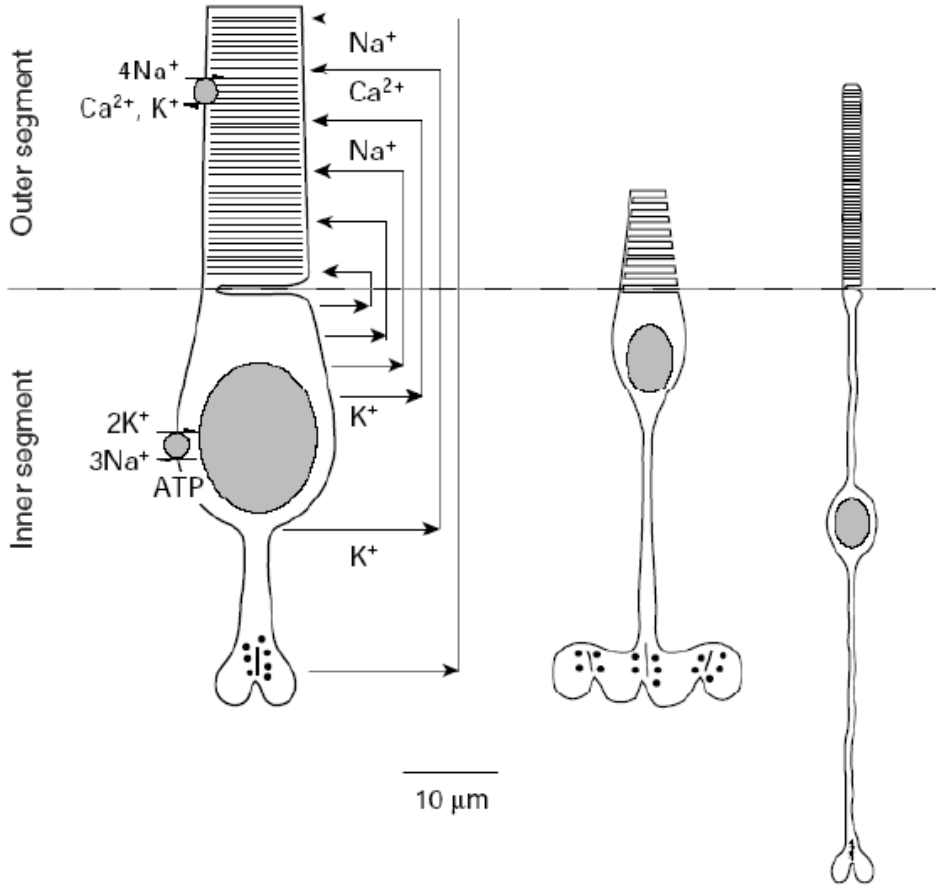

Figure 2.3. Structure of rods and cones and nature of the circulating current. A salamander rod, a salamander red-sensitive cone, and a mammalian rod are shown from left to right. (Pugh and Lamb, 2000)

Besides morphological differences, the rods and cones function differently. Cone

photoreceptors function well in bright light and are adapted to detect colors, while rod photoreceptors are more sensitive to dim light. In humans, there are three types of cones that respond to blue (short wavelength), green (medium wavelength), and red (long-wavelength) light.

The outer segment of a rod photoreceptor (ROS) contains a pile of disc membranes stacked along the medial axis of the ROS, with consistent intervals of about 28 nm. This layout allow for increased probability of capturing a photon traveling axially down the ROS.

2.1.2 The Circulating Current

In dark-adapted conditions, cGMP-gated channels in the rod outer segment permeate an inward ionic flow. The flow is composed mainly of Na^+ (about 85%-90%) for the reason that Na^+ being the predominant external ion, while Ca^{2+} ions carry the remaining 10%-15% due to the high permeability of the channel to Ca^{2+}. There is an additional contribution of Mg^{2+}, but usually quite small (Nakatani and Yau, 1988). At a certain Ca^{2+} level, a tonic release of glutamate from the rod synaptic terminal is sustained to send information to the second-order neurons of bipolar and horizontal cells.

A large portion of this cGMP-gated current is balanced by outgoing currents carried by K_x channels in the inner segment plasma membrane. Together, the influx and the balancing efflux current form a loop (Figure 2.3) that is commonly referred to as the ‘circulating current’. In dark resting condition, this current loop is also called the ‘dark current’. Figure

2.4 illustrates recordings of the circulating current from a Salamander rod, a human rod and a Salamander cone.

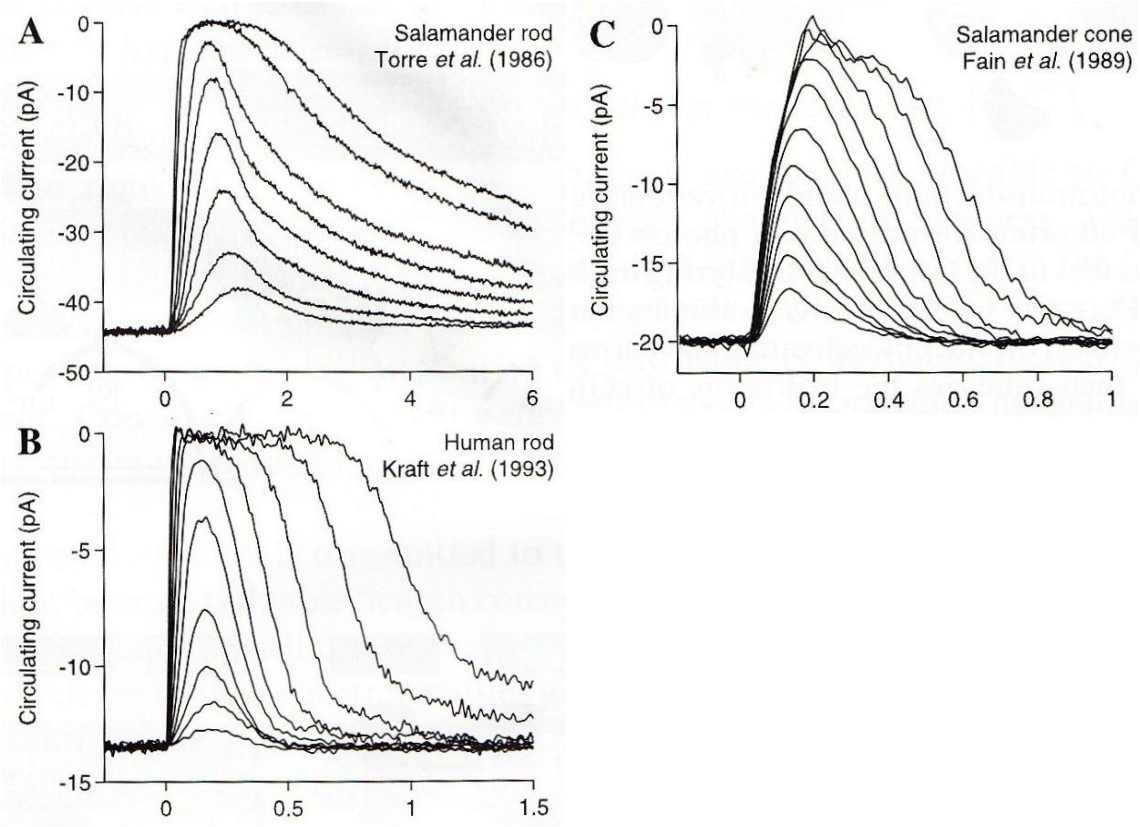

Figure 2.4. Recordings of the circulating current from (A) a Salamander rod, (B) a human rod and (C) a Salamander cone (Torre et al., 1986; Fain et al., 1989; Kraft et al., 1993).

The electric response generated by the rod photoreceptor when given a light stimulus is initiated from the closing of cGMP-gated channels in ROS, and is a transient suppression of the circulating current. In vertebrate single rod photoreceptors, the magnitude of the circulating current is usually in the range of 20~70 pA (Baylor et al., 1984; Cobbs and Pugh, 1987; Kraft et al., 1993; Miller and Korenbrot, 1994; Chen et al., 1995; Schneeweis and Schnapf, 1995; Xu et al., 1997). Table 2.1 summarizes the typical outer segment parameters

and dark resting electrical properties of photoreceptors in four animal species. The peak amplitude of receptor response increases with light flash intensity, until the circulating current reaches its minimum value near zero. The time to reach peak is ~200 ms for mammalian with dim flashes, and shorter with bright flashes (Torre et al., 1986; Matthews et al., 1990; Kraft et al., 1993). The ERG a-wave corresponds to the beginning portion of this receptor response.

Quantity	Symbol	Unit	Rods				Cones		
			Salamander	Toad	Primate	Mouse	Salamander	Turtle	Primate
Outer segment parameters									
Wavelength of maximum absorption	λ_{max}	nm	500	500	500	500	610	650	565
Length	L	μm	22	60	25	20	8	15	13
Diameter (base, tip)	d	μm	11	6	2	~2	4, 2.5	2.5, ~1	3, ~1
Envelope volume	V_{tot}	μm^3	2000	1800	40	30	70	30	30
Cytoplasmic volume	V_{cyto}	μm^3	1000	900	20	15	35	30	15
Temperature	T	C	22	22	37	37	22	22	37
cGMP-activated current (in dark)	J_{cG}^D	pA	−70	−40	−50	−20	−50		−40
$Na^+/Ca^{2+},K^+$ exchange current (in dark)	J_{ex}^D	pA	−4	−3	−2	−1	2		
Typical whole-cell electrical properties									
Resting potential (in dark)	V_m	mV	−40		−37		−40	−40	−45
Time-to-peak (dim flashes)	t_{peak}	ms	700	1500	200	240	170	100	50
Flash sensitivity	S_F^D	pA/Φ	0.2	1	0.7	0.4	0.03		0.02
(at t_{peak}, in darkness)		mV/Φ	0.06		1.2		0.03	0.025	0.005
Capacitance	C	pF	20	20		1	70	40	
Time constant (dark)	τ_m	ms	20	20	1	1	50	5	3
References			[48–50]	[34,51]	[38,52,53]	[39,40,54]	[50,55–57]	[58–60]	From [61] as cited in [62]; [63,64]

[a] *Notes*: 1. Values given are representative of measurements in the literature.
2. Where whole-cell recording data are not available, we have used estimates based on suction-electrode recordings, and assumed a suction electrode collection efficiency of 2/3.
3. Primate cone anatomical properties are systematically dependent on distance from the fovea; the parameters given are applicable for the shorter but wider peripheral cones. The cited references illustrate and discuss this variation in cone anatomy.

Table 2.1. Typical outer segment parameters, and dark resting electrical properties of vertebrate rods and cones (Pugh and Lamb, 2000).

2.1.3 Phototransduction Process

When a photon comes in, it is absorbed in the rod outer segment and an electric response is generated. The process is called phototransduction, and it consists of complex molecular mechanisms. As illustrated in Figure 2.5, the capture of a photon will cause formation of

Meta II rhodopsin (R*) that catalyzes the exchange of GDP for GTP on the α-subunit of the G-protein. Activation of the G-protein cascade leads to activation of cGMP phosphodiesterase (PDE) and raises the level of cGMP hydrolysis. As the cytoplasmic concentration of cGMP reduces in the vicinity of photon absorption, the cGMP-gated channels begin to close locally within that region and induce hyperpolarization of the rod cell. This will serve to inhibit glutamate release from rod synaptic terminal.

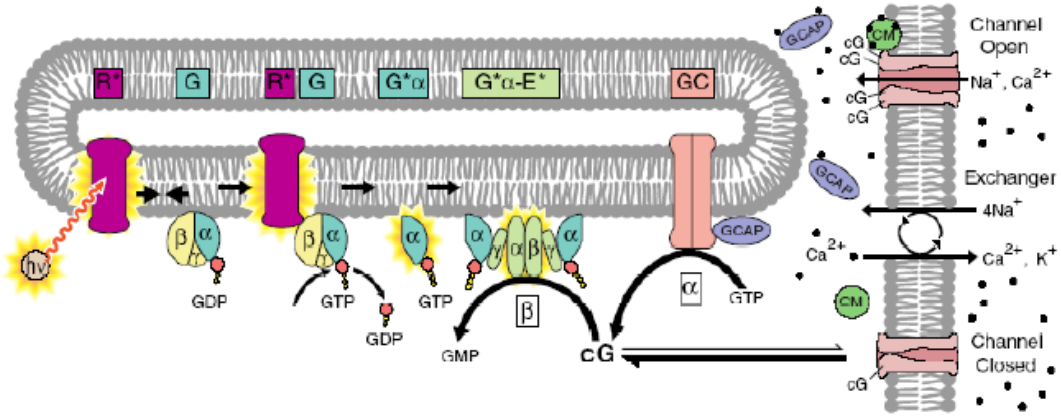

Figure 2.5. Schematic drawing of activation steps of phototransduction cascade in vertebrate photoreceptors (Pugh and Lamb, 2000).

Following excitation of the visual cascade system, inactivation steps and cGMP re-synthesis take place to return the photoreceptor back to its dark resting state. Illustrated in Figure 2.6 is the inactivation process of the rod phototransduction.

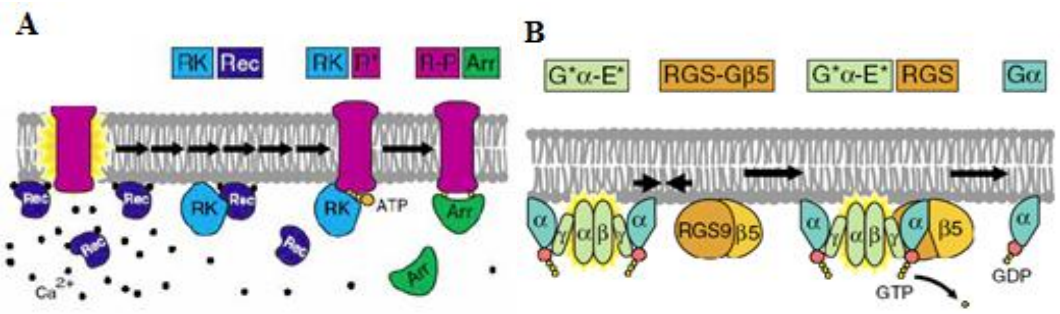

Figure 2.6. Inactivation steps of phototransduction cascade. (A) Inactivation of R*. (B) Inactivation of G*-E*. (Pugh and Lamb, 2000)

After the cell hyperpolarizes, cytoplasmic free Ca^{2+} concentration continues to decline as a result of continuous extrusion by Na^{+}/Ca^{2+}, K^{+} exchangers and the lack of input flux. The Ca^{2+} ions that are bound to recoverin (Rec) to form Rec-2Ca complex are released, and the complex is dissociated from rhodopsin kinase (RK). Then arrestin binds and this stops the R* activity. Transducin re-associates with β- and γ-subunits and comes back to its inactive form, which also restores PDE to its inhibited state. Lower Ca^{2+} concentration leads to activation of guanylate cyclase, and cGMP-gated channels reopen with elevated cGMP concentration to help repolarize the cell. In turn, the intracellular free Ca^{2+} concentration is increased and at the same time returns guanylate cyclase to its original level of activity (Buck and Axel, 1991; Zufall and Leinders-Zufall, 1998; Mombaerts, 1999).

2.2 Electroretinogram (ERG) and Existing Models

2.2.1 The Electroretinogram (ERG)

It was first discovered in 1865 that there was an electric response from the eye to a light

stimulus when electrodes were placed at the front and back of a frog eye (Perlman, 2005). The recordings were, however, not really comprehended until 1870 when Holmgren proposed his explanation of the phenomenon (Holmgren, 1870).

In 1908, the ERG was first reported to consist of three waves: a-wave, b-wave and c-wave (Einthoven and Jolly, 1908). The view point is that light causes a series of processes that would give rise to products A, B and C, each of which is indicated by a respective waveform. In 1911, a different speculation is provided by Piper (Piper, 1911). It was proposed that all components of ERG last for the duration of the overall electric response. Figure 2.7 (A) shows

Granit (1933) published his work that suggests ERG to be composed of three parts: P-I, P-II and P-III (Figure 2.7 (B)).

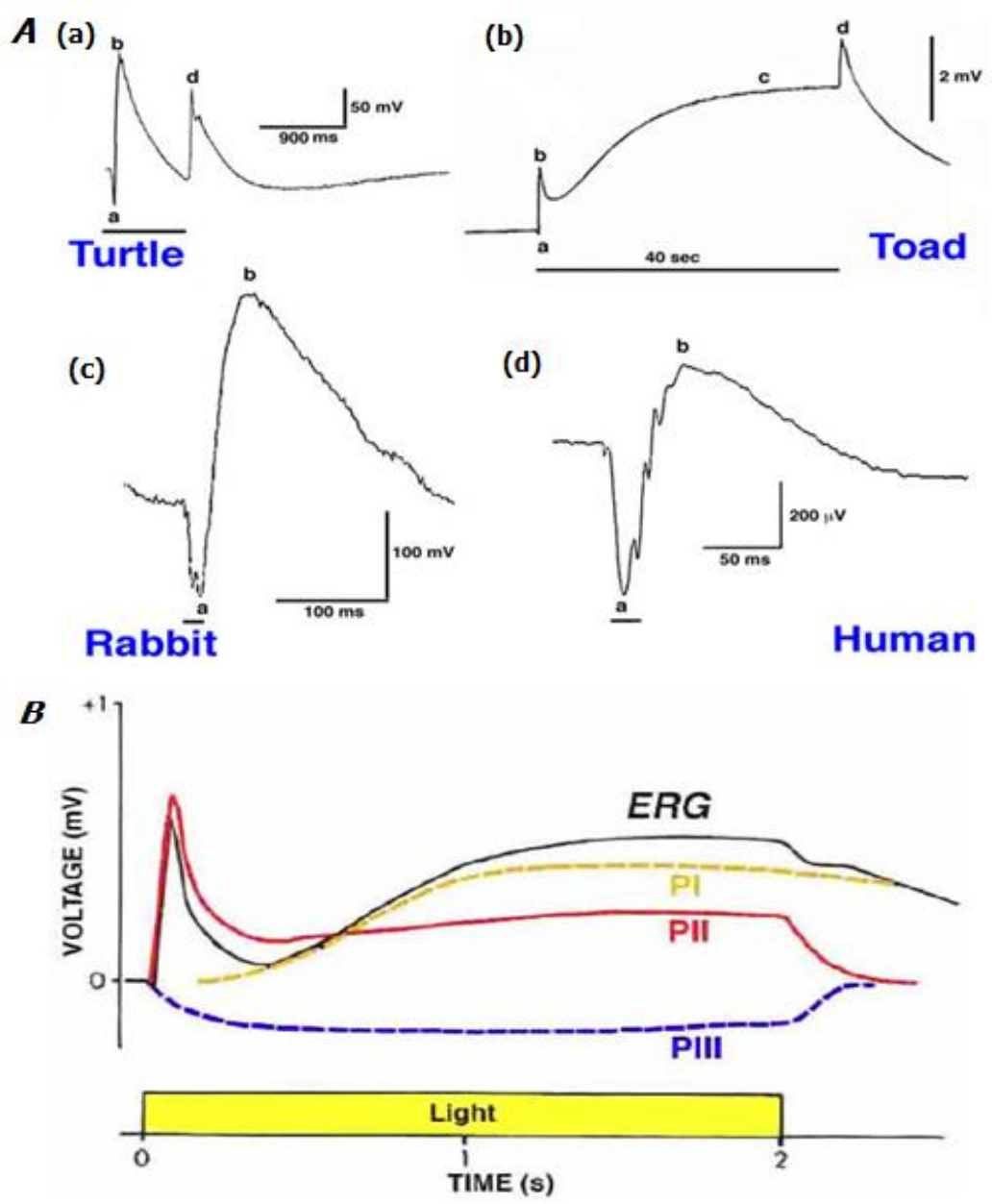

Figure 2.7. (A) ERG responses of (a) turtle Pseudemys scripta elegans elicited by a 900ms light stimulus in order to separate the a-wave and b-wave from the d-wave, (b) bullfrog elicited by a long (40sec) light stimulus in order to show the c-wave in addition to the a-, b-, and d-wave (Oakley, 1977), (c) a rabbit to a flash (20ms) of white light, and (d) a human as typically recorded in clinic. Calibration bar are denoted separately for each ERG response. (B) ERG recording of a cat to two second light stimulus. PI, PII and PIII were separated by increasing depth of anethesia (Granit, 1933).

As for origins of ERG a-, b- and c-waves, the a-wave is considered to be solely generated

by photoreceptor cells, while the b-wave is thought to come from bipolar cells postsynaptic to the photoreceptors. The c-wave is originated in the pigment epithelium.

Besides these major waves, other minor components have been identified since, such as the d-wave and oscillatory potentials, depending on the recording conditions. These works are still the basis for ERG analysis today.

In the measurement of electroretinogram (ERG), the ERG a-wave, which includes the leading edge of the electrical response currents from photoreceptors, is important for assessment of retinal phtoreceptor cell functions. The clinical diagnosis of retinal diseases and degenerations are mainly made by evaluations of both a- and b-waves. It allows testing of quantitative hypothesis of retinal function, and helps to understand the underlying physiological mechanisms.

2.2.2 Background of Photocurrent Models

Many analytical approaches have been proposed to describe the a-wave. Among them, there are two major models: one proposed by Hood and Birch (1990), and the other by Lamb and Pugh (1992), which was later modified by Nikonov et al (1998).

The Hood and Birch model is a statistical fitting to the a-wave response with a linear and a nonlinear component. It supports the notion that the a-wave is a response of the rod photocurrent. The model, however, lacks an explicit physical or biological basis and does not provide much insight into the underlying biochemical mechanisms.

The second model was originally proposed by Lamb and Pugh (1992), and was later modified in 1998 by Nikonov et al (1998). The model was developed to represent the reaction kinetics of phototransduction at the molecular level. It was first applied to salamander rod response, and proved to fit human ERG a-wave as well (Smith and Lamb, 1997). The major limitations of the model are the exclusion of the inactivation and recovery stage and oversimplification of the dependence of the circulating current on the ion activities.

2.3 Ion Channels in Rod Photoreceptors

As illustrated in the previous section, the rod photoreceptor cells can be viewed morphologically as having an outer segment and an inner compartment. The inner compartment consists of an inner segment proper, the soma, a short axon, and a nerve ending (Molday and Kaupp, 2000). Both the outer segment and the inner compartment contain ion channels participating in the ionic activities that shape the light response of photoreceptor cells.

The cGMP-gated channels are exclusively located on the surface of the outer segment, and can be closed by incoming light (Baylor and Lamb, 1982). In the ROS, there is also a class of proteins contributing to ion permeation, which are the Na^+/Ca^{2+}, K^+ exchangers (NCKX) (Schnetkamp, 1989; Lagnado and McNaughton, 1990; Schnetkamp, 1995; Finn et al., 1996; Molday and Molday, 1998; Molday and Kaupp, 2000). In the inner compartment of a rod photoreceptor, there is the Na/K ATPase, and at least five types of ion conductances

have been identified. These channel types include: (1) voltage-gated K^+ channel; (2) hyperpolarization-activated channel, commonly referred to as I_h channel (also HCN_x channel standing for hyperpolarization- and cyclic nucleotide-activated channel of unknown subtype), which is permeable to many cations; (3) voltage-gated Ca^{2+} channel; (4) Ca^{2+}-activated K^+ channel and (5) Ca^{2+}-activated Cl^- channel. Besides the five types of channels above, a GMP-gated channel type has also been identified, but only exists in the presynaptic terminals of the cone photoreceptor synapse. A schematic drawing of the rod photoreceptor and its ion channels is shown in Figure 2.8. In the following, some physiological properties of these channels are reviewed and their functions in shaping the light response discussed.

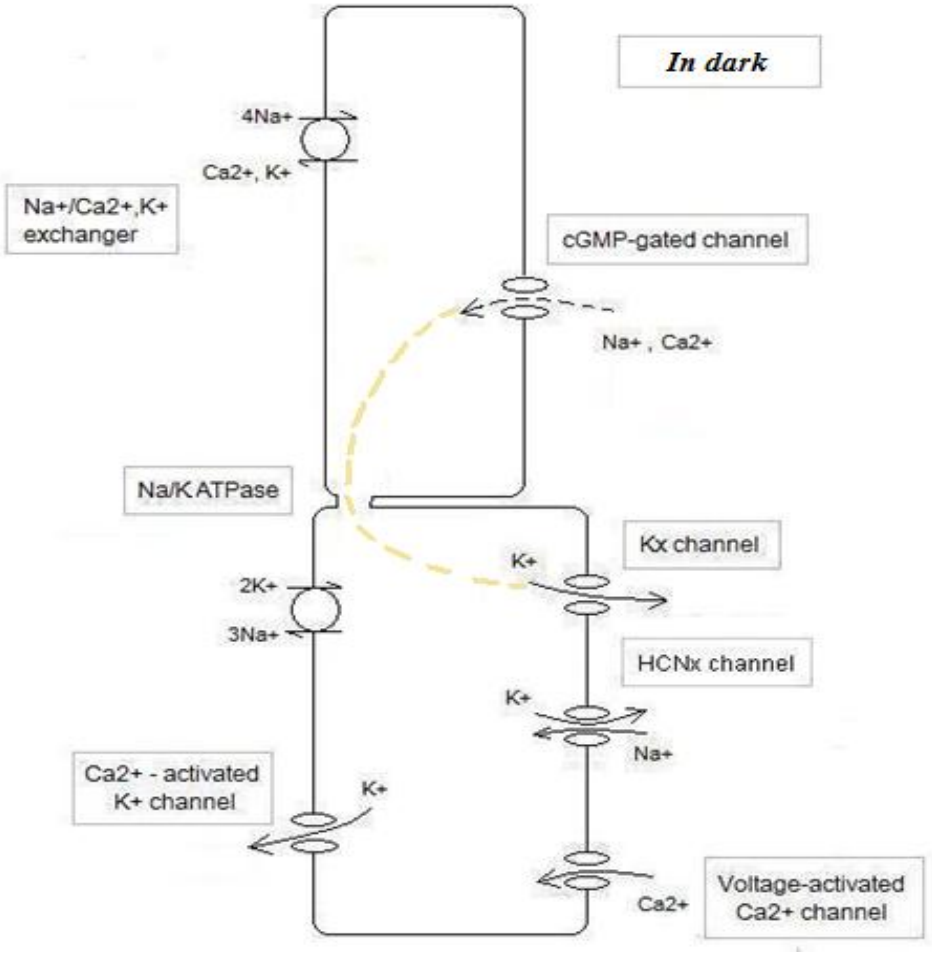

Figure.2.8. Channel inventory of a rod photoreceptor cell. HCN_x, stands for hyperpolarization- and cyclic nucleotide-activated channel of unknown subtype. Arrows indicated direction of currents in dark resting state. Trend line in yellow color indicates the dark circulating current traveling from cGMP-gated channels in outer segment to K_x channels in inner compartment.

2.3.1 Outer Segment Ion Channels

2.3.1.1 Cyclic GMP-gated Channels of Photoreceptors

The cyclic GMP-gated channel (cGMP-gated channel) has a central role in the process of phototransduction, and controls the major inward ionic flow of the dark circulating current that goes through the rod outer segment.

There have been many studies on the cGMP-gated channel in rod photoreceptor cell, including electrophysiological recordings of membrane patches and isolated rod outer segments, and biochemical studies of membrane vesicles in the outer segment. It has been found that the channel is activated by cGMP and, when cGMP concentration is within 20-80 μM, the channel reaches its half-maximum-activation point (Mixon et al., 1995; Wall et al., 1995; Sondek et al., 1996; Sprang, 1997). Even with small changes in free cGMP concentrations, which are common in the phototransduction process, the cGMP-gated channel is able to respond. It has also been observed that the channel can be activated by cyclic AMP, but a high cAMP concentration is required, and the maximum current is less than 30% of that activated by cGMP (Lamb and Pugh, 1992; Hamm, 1998; Iiri et al., 1998). In dark-adapted conditions, the free cGMP concentration in the rod outer segment is kept at a relatively high level, making the cGMP-gated channel remain open in the dark.

In dark and under normal physiological conditions, the inward current permeated by cGMP-gated channels is composed of many types of monovalent and divalent cations (Snyder and Menzel, 1975; Enoch and Tobey, 1981; Pugh and Lamb, 2000). According to the current literature, approximately 85-90% of the current is carried by sodium ions, 10-15% by calcium ions, and a very small portion comprising ions such as Mg^{2+} (Nakatani and Yau, 1988).

Immunocytochemical methods and patch clamp recordings have been applied to study the distribution of cGMP-gated channels on the rod cell membrane. The results from

immunocytochemical methods have shown that the cGMP-gated channels are predominantly, more likely to be exclusively, located in the plasma membrane of rod photoreceptor outer segment (Harosi and Malerba, 1975; Aho et al., 1993). From patch clamp recordings of excised membrane patches of the rod photoreceptor, findings show that the channels are densely located in the rod outer segment membrane and few are present in the inner compartment of rod (Chen et al., 1995).

Through biochemical measurements (Aho et al., 1993), and also whole cell noise measurements and single cell recordings (Lagnado and McNaughton, 1990; Schnetkamp, 1995; Sprang, 1997), the density of cGMP-gated channels in the rod plasma membrane has been estimated at around 500 channels/μm^2.

2.3.2 Inner Compartment Ion Channels

2.3.2.1 K_x Channels

Under dark conditions, there are ionic conductances in the inner compartment that allow an outward K^+ current, balancing the dark inward current through cGMP-gated channels in the outer segment membrane (Beech and Barnes, 1989). This outward K^+ current is often symbolized as I_{Kx}, and the corresponding channels as K_x channels. Beech and Barnes (1989) observed that these K_x channels are closed by hyperpolarization but are non-inactivating, and they open relatively slowly when hyperpolarized below -50 mV. In addition, the voltage point of K_x activation will change to much more positive values with the presence of external Ba^{2+}.

However, acetylcholine does not suppress I_{Kx}. Currents of similar properties were also identified for cone photoreceptors (Barnes and Hille, 1989; Maricq and Korenbrot, 1990).

In the work by Barnes (1994), the physiological function and characteristics of currents through K_x channels and hyperpolarization-activated (I_h) channels were investigated and described. The relation between channel activation and membrane voltage for these two types of channels is illustrated in Figure 2.9.

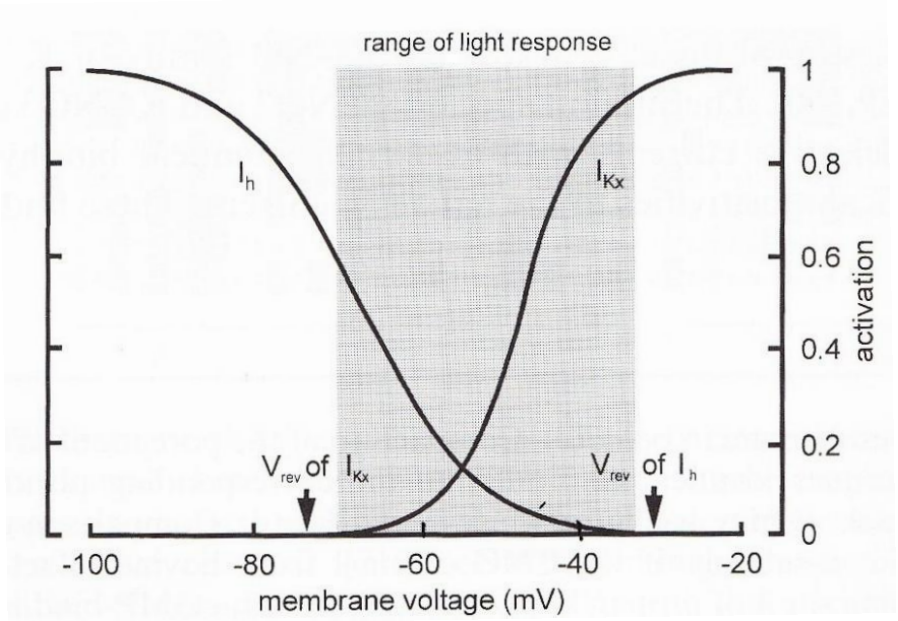

Figure 2.9. Activation curves of K_x and I_h channels in rod photoreceptor cell (Barnes 1994).

The K_x channels in the inner compartment have steep voltage-dependence for activation. In the dark, the membrane potential rests at ~ -35 mV and the K_x channels are activated to a large extent. Flux driven by ion concentration gradients and membrane voltage thus produces a relatively large outward K^+ current. This current, together with the inward current through

the cGMP-gated channels in the outer segment, will balance and largely set the resting membrane voltage in the dark.

Hyperpolarization will induce deactivation of K_x channels. From around -40 mV to 55mV, the channel activation ratio is particularly sensitive to changes in membrane voltage, and should be most effective in producing large light-evoked hyperpolarizations. The reversal potential V_{rev} of K_x channel is roughly -75 mV, where the channel open ratio reduces to less than 2% of the fully activated state. At more hyperpolarized membrane voltages (Vm < -60 mV), current through K_x channels begins to disappear because of reduced driving forces and closing of K_x channels.

2.3.2.2 Hyperpolarization-activated (I_h) Channels

In the work by Fain et al. (Fain et al., 1978), a conductance on rod photoreceptor membrane activated by hyperpolarization was first observed and described. This work expanded a previous model of the receptor response and explained many of the complexities in the response. When given high-intensity light, the membrane is quickly hyperpolarized and then followed by relaxation to a less-negative value. Lower light intensities cause smaller hyperpolarizations and the initial spike does not show. Fain and coworkers' experiments showed that, when the retina is superfused with a Ringer solution containing cesium chloride, the membrane voltage drop is much attenuated and the receptor response lacked fast decay. Compared to that at lower light intensities, Cs^+ showed no influence on the shape of the

response (Figure 2.10). Fain and coworkers concluded that a Cs^+-sensitive conductance on the rod membrane is activated by light-evoked hyperpolarization, and suggested this conductance to be largely responsible for the rapid decay of the rod potential under high intensity light. Later studies using the voltage-clamp technique on photoreceptors with and without the outer segment showed that the current activated by hyperpolarization is inward in the inner compartment and is responsible for most of the depolarizing drop afterwards (Bader et al., 1979; Bader et al., 1982; Baylor et al., 1984; Hestrin, 1987).

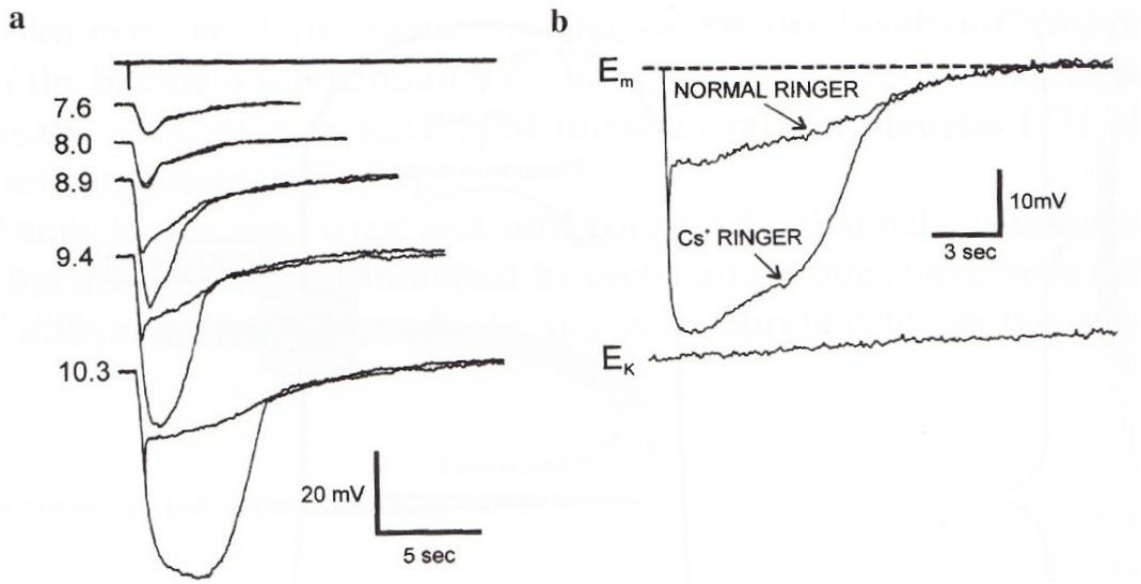

Figure 2.10. Cs^+ affects rod photoresponse waveform (Fain, Quandt et al. 1978)

Hyperpolarization-activated channels are not very common in the family of voltage-gated channels, as most channel types, e.g., Na^+, K^+ and Ca^{2+} channels, are activated by depolarization,. The I_h channel in the photoreceptor, although sharing many similar properties with the I_h channels found in frog muscle and heart muscle, differs from the major

channels in the photoreceptor cell.

In the rod photoreceptor, the mid-point voltage of activation for I_h channels is around ~-67 mV (Hestrin, 1987), and the reversal potential is near -30 mV in a normal standard salt solution. This suggests that the I_h channels are not activated in the dark resting state, and do not play a role in the V_m in dark, which is normally from -30 mV to -40 mV.

The I_h channels are multi-ion pores and weakly selective between Na^+ and K^+ ions (Hestrin, 1987). Relative permeability ratios P_x/P_K for I_h channels are: Tl^+ (1.55) > K^+ (1) > Rb^+ (0.55) > Na^+ (0.33) > Li^+ (0.02) (Wollmuth and Hille, 1992). The permeability ratio P_{Na}/P_K depends on external potassium concentration $[K^+]_e$. The ratio changes from 0.2 to 0.3 when external potassium increases from 2.0 mM to 10.0 mM. Particularly, in the absence of external potassium, little or no Na^+ ions can be permeated through the channel. It was observed that in solutions containing Na^+ but no K^+, I_h channels gate normally, suggesting that Na^+ might permeate very slowly (Wollmuth, 1995). Changes in $[K^+]_e$ do not affect the voltage-conductance relationship or channel kinetic parameters (Hestrin, 1987). As a consequence, current through I_h channels is composed mainly of Na^+ and K^+ ions at physiological ion concentrations, and the direction of current reverse roughly at V_m > -60 mV. Hence, during a saturating light response, I_h channels permeate an inward current that is predominantly composed of Na^+ ions (Wollmuth and Hille, 1992).

From the structure of I_h channels in rod, the I_h channels feature a cyclic nucleotide-binding motif (Aiba et al., 1982; Takio et al., 1984; Titani et al., 1984; Ludwig et

al., 1990), but have not been shown to be modulated by cyclic nucleotides.

In Figure 2.8, the activation curve of the I_h channel is illustrated together with the activation curve of the K_x channel, which shows opposite voltage dependence. The curves and reversal potential V_{rev} are positioned at two opposite ends of the operation range. The half-point activation potential of I_h channels is around -67 mV, and the reversal potential is close to -32 mV, confirming that I_h channels do not contribute to the resting membrane voltage in the dark. The I_h channels show little activation from the dark resting voltage (around -30mV ~35mV) to -40mV ~ -50mV and thus, produce very small I_h currents. When the rod photoreceptor is hyperpolarized to below -50 mV, I_h activation becomes steeply voltage-dependent and the channels carry a depolarizing inward current of Na^+ and K^+ primarily. As a result, the I_h channel in rod operates to resist the photoreceptor hyperpolarization in response to light.

2.3.2.3 Voltage-activated Ca^{2+} Channels

The Ca^{2+} channels located at the presynaptic terminal of the rod photoreceptor are voltage-dependent. A portion of these Ca^{2+} channels are held open at the dark resting voltage. This sustains a tonic release of glutamate from the synaptic terminal to the second-order neurons of bipolar cells and horizontal cells.

The activation threshold of Ca^{2+} channels is around -45 mV (Bader et al., 1982). Hence, the Ca^{2+} channels are closed when rod photoreceptor hyperpolarizes to below -45 mV, and

synaptic transmissions are ceased. The voltage-conductance relationship is steep between -35 mV to -15 mV. It was observed that the Ca^{2+} channel open ratio changes e-fold with each 6 mV change in membrane potential (Bader et al., 1982). As for synaptic transmission of glutamate, 2.1 mV of depolarization in membrane voltage can cause transmission to increase e-fold (Attwell et al., 1987). This results in a steep non-linear input-output relation of rod synapse in that small changes from the resting voltage modulate glutamate release while V_m lower than ~ -45 mV ceases the transmission. Furthermore, 3 or 4 Ca^{2+} ions needs to bind to trigger exocytosis of glutamate from the presynaptic terminal.

2.3.2.4 Ca^{2+}-activated K^+ Channels and Ca^{2+}-activated Cl^- Channels

It was observed in experiments that in the inner compartment of photoreceptor cells there were two different Ca^{2+}-dependent ionic outward flows (Bader et al., 1982; Maricq and Korenbrot, 1988; Barnes and Hille, 1989; Maricq and Korenbrot, 1990). These two currents are permeated by the Ca^{2+}-activated K^+ channels and Ca^{2+}-activated Cl^- channels respectively.

Compared to the other inner compartment ion channels, the properties and functions of these two channels are less known. However, it is possible that the two types of channels can provide further depolarization when re-activated by the influx of Ca^{2+} ions through the opening of voltage-activated Ca^{2+} channels, and when voltage-activated Ca^{2+} channels are closed by hyperpolarization, they can serve to repolarize the cell (Maricq and Korenbrot,

1988).

2.4 Progressive Retinal Atrophy (PRA) in Abyssinian Cats

Progressive retinal atrophy (PRA) is a group of genetic diseases of slowly progressive retinal degeneration. It usually starts with decreased vision in the dark, and causes progressive vision loss that eventually leads to blindness.

The PRA has been described in Abyssinian cats (Narfstrom, 1983b; Narfstrom and Nilsson, 1983; Narfstrom, 1985), and was found to be transmitted by a simple recessive gene (Narfstrom, 1983). The disease gene is found to be localized to the connecting cilium of rod photoreceptor cells, and colocalized with proteins that are critical for the frequent regeneration of rod photoreceptor outer segment discs (Pazour et al., 2002; Pazour and Rosenbaum, 2002). At early stages of the disease, rod outer segment discs in the periphery can be found disorganized or vacuolated. As the disease progresses, the lesions spread throughout the retina, and both rods and cones become involved. At later stages, cell death of both rods and cones can be observed (Narfstrom & Nilsson, 1986).

In affected individual Abyssinian cats that are at early stages of the disease, a clearly noticeable vacuolization can be observed in the basal part of rod outer segment. This region is near the connecting cilium, and is the place where new outer segment discs are formed (Figure 2.11) (Narfstrom, 1985). The findings suggest early abnormalities in the transport and distribution of phototransduction and/or structural proteins through the connecting cilia

in the diseased cat model and photoreceptor degeneration.

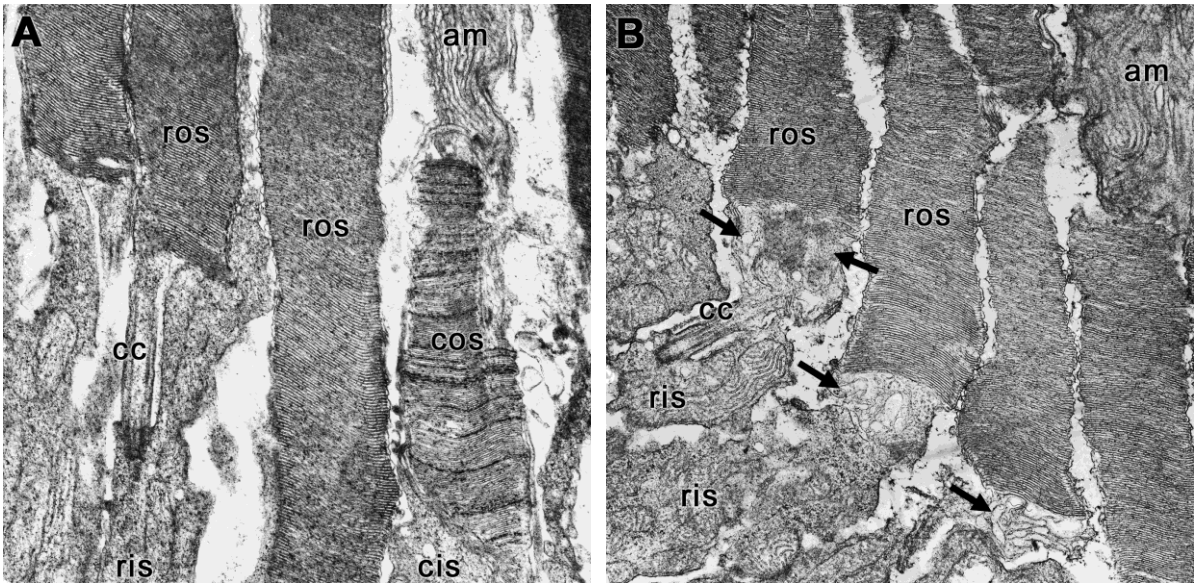

Figure 2.11. Electron micrograph of outer retina showing photoreceptor outer and inner segment of (A) normal Abyssinian cat and (B) young affected rdAc cat. Note abnormalities at the base of the rod outer segments near the connecting cilium in (B). Membranes are not formed as in the normal cat, instead there are vacuolization and degeneration (arrows) of membranes in the affected retina. Am, apical microvilli of the retinal pigment epithelium; ros, rod outer segments; ris, rod inner segments; cos, cone outer segments; cis, cone inner segments; cc, connecting cilium of the photoreceptor (Menotti-Raymond et al., 2007).

CHAPTER 3

MODEL DEVELOPMENT

3.1 Proposed Model for Photoreceptor Response

To improve the use of electroretinogram (ERG) and the understanding of the photoresponse process, a mathematical model was developed based on the ionic activities during the photoresponse process and experiment data. In this model, three major ion species are included, Na^+, K^+ and Ca^{2+}, which are most active during the photoresponse process and are responsible for most of the response waveform. Other ion species such as Cl^- and Mg^{2+} also participate in the physiological process; however, their effects on the ionic activities are much smaller than those of the three main ion species, and are thus not included in the model. As a result, the ion channels considered in the model are cGMP-gated channels, K_x channels, I_h channels, voltage-activated Ca^{2+} channels and Ca^{2+}-activated K^+ channels (Figure 3.1).

3.1.1 Model Structure and Corresponding Bondgraph Representation

The membrane voltage is affected by the net charges accumulated inside the cell body. Instead of modeling the cell membrane plus the conducting inner and outer media as a two-plate capacitor, we view the cell itself as an absolute capacitor in the outside media. There are two major ways to charge this capacitor: one is ion flow though ion pumps and exchangers; and the other is ion flow though ion channels driven by concentration gradients

and electrical potential differences across the cell membrane.

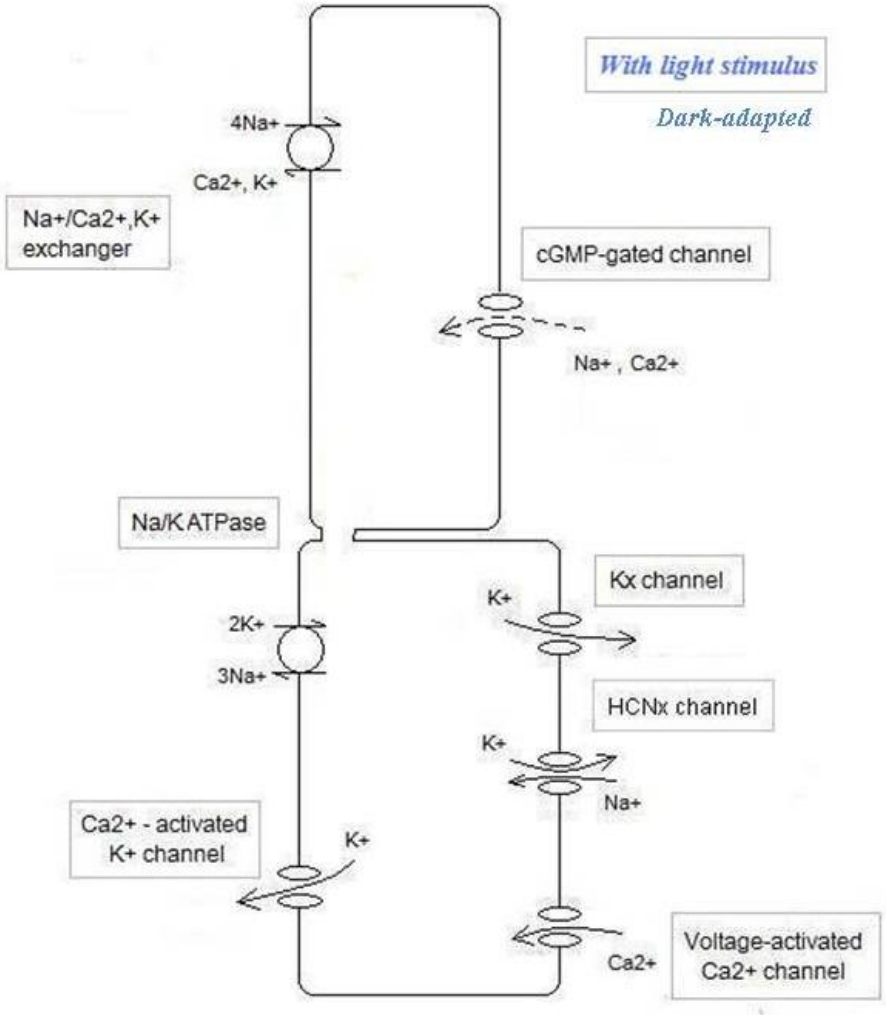

Figure 3.1 Channel inventory of a rod photoreceptor cell.

Figure 3.1 illustrates the major channels of a vertebrate rod photoreceptor cell. Arrows mark the permeating currents and their directions. The outer segment plasma membrane of the rod photoreceptor cell holds the Na/Ca-K exchanger, which extrudes Ca^{2+} and K^{+} from the outer segment in exchange of Na^{+}. In the inner compartment, the Na^{+}/K^{+}-ATPase transports Na^{+} out and K^{+} in.

A bond graph is originally a graphical representaion of a physical dynamic system. This modeling approach has been applied to many biological systems as well (Allen, 1978; Imai, 1996; Grell et al., 1999; Lo et al., 2004). Here, the power flows and mass flows in the system can be represented with bond graphs in Figures 3.2 - 3.4.

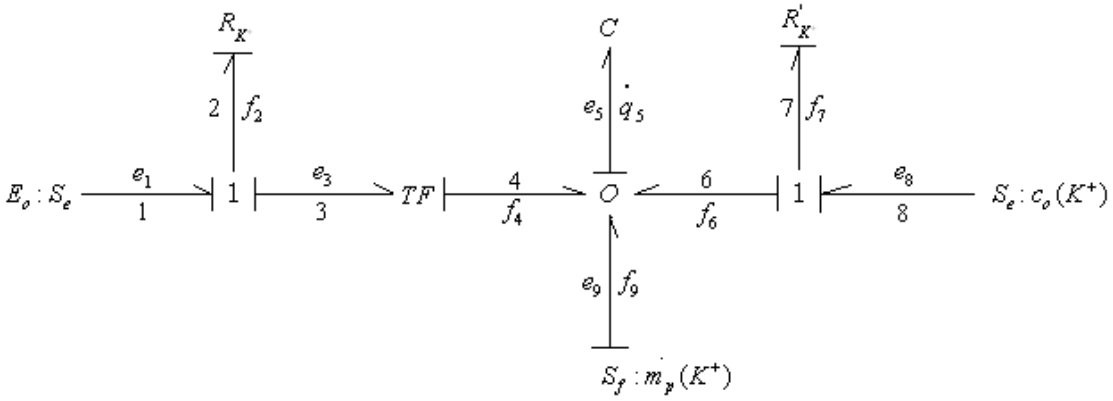

(A) Transport of K^+ ions

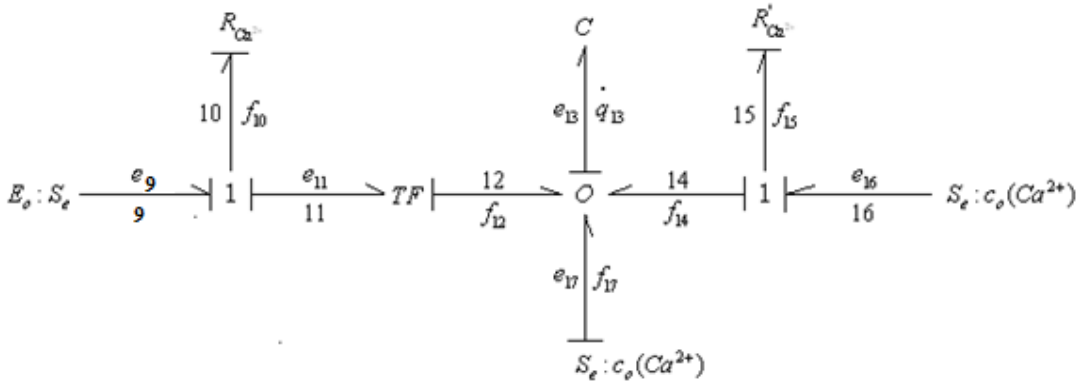

(B) Transport of Ca^{2+} ions

Figure 3.2. Bond graphs for K^+ and Ca^{2+} ion transport in the inner compartment. S_e – effort source, c_0(Ca^{2+}) – concentration of Ca^{2+}, C – capacitor, R – resistor, S_f – flow source, TF - transformer, $\dot{m}_p$ – exchange rate of K^+ through Na/K ATPase, e_n(n=1,2, …, 16) – effort, f_n (n=1,2, …) – flow, q_n (n=1,2, …, 16) – generalized displacement (charge).

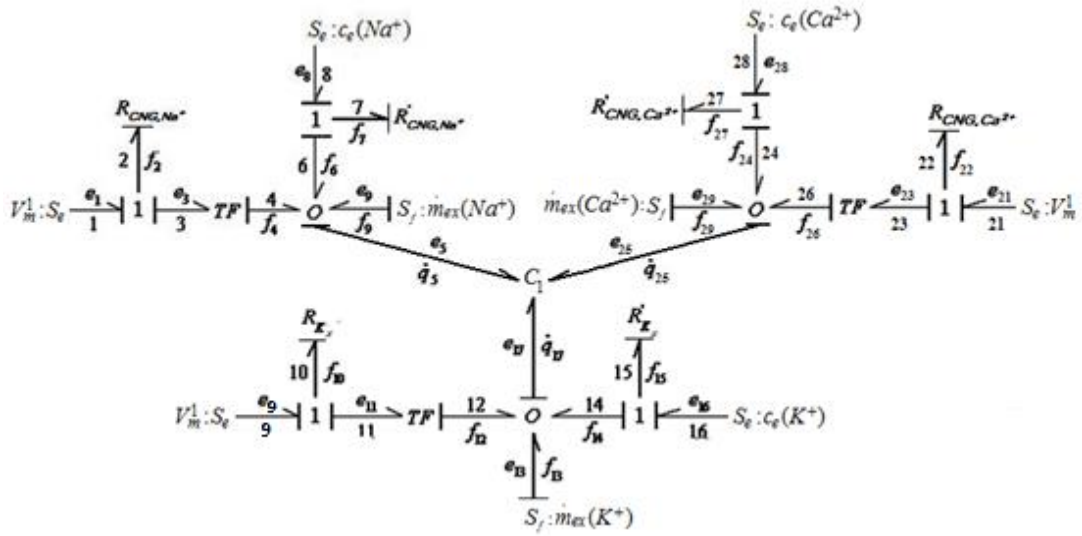

Figure 3.3. Bond graph of ionic activities inside the outer segment of a rod photoreceptor cell. S_e – effort source, $c_0(Ca^{2+})$ – concentration of Ca^{2+}, C – capacitor, R – resistor, S_f – flow source, TF - transformer, $\dot{m}_{ex}$ (S) – exchange rate of ion species S through Na^+/Ca^{2+}, K^+ exchanger, e_n(n=1,2, …, 29) – effort, f_n (n=1,2, …) – flow, q_n (n=1,2, …, 29) – generalized displacement (charge).

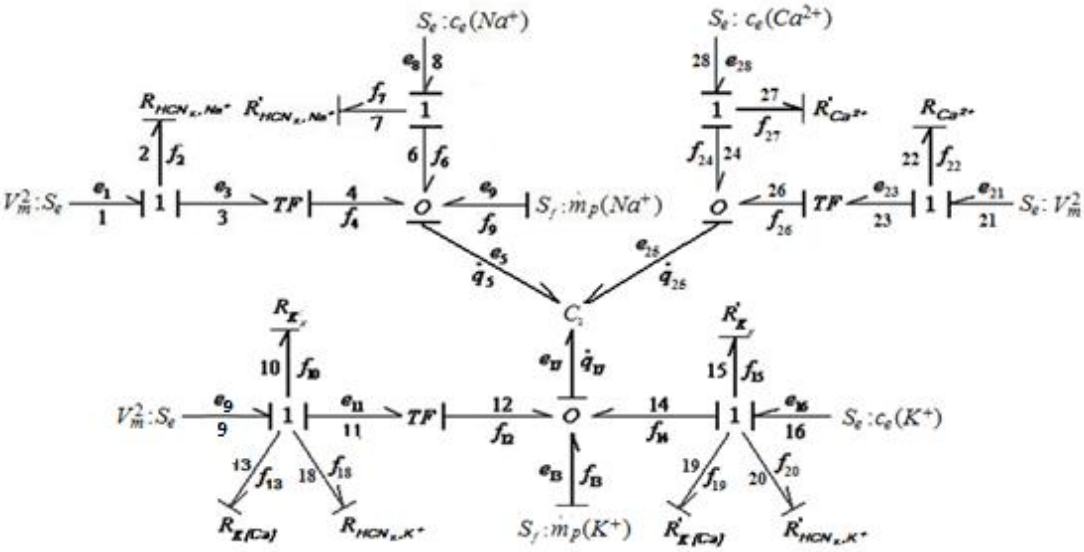

Figure 3.4. Bond graph of ionic activities inside the inner compartment of a rod photoreceptor cell. S_e – effort source, $c_0(Ca^{2+})$ – concentration of Ca^{2+}, C – capacitor, R – resistor, S_f – flow source, TF - transformer, $\dot{m}_p$ – exchange rate of ion species S through Na/K ATPase, e_n(n=1,2, …, 28) – effort, f_n (n=1,2, …) – flow, q_n (n=1,2, …, 28) –generalized displacement (charge).

In the bond graphs above, R_S stands for the electric resistance of the corresponding channel S, and R'_S represents the resistance to material diffusion through channel S. The values for R_S and R'_S, and the relationship between them will be discussed in the next section. Also, a method to compute the membrane voltage (V_m) based on Gauss's law will be proposed.

From the bond graphs in Figure 3.2 the following set of equations are derived describing the mass flows and energy flows in the inner compartment. Equations that describe activities in the outer compartment can be derived similarly.

$$e_1 = E_o, \quad e_2 = e_1 - e_3$$

$$f_2 = f_1 = f_3, \quad f_2 = \frac{e_2}{R_{K^+}}$$

$$f_4 = \frac{f_3}{q_e \cdot N_a}, \quad f_9 = \dot{m}_{p,K^+}, \quad f_7 = \frac{e_7}{R'_{K^+}} = f_6 = f_8$$

$$e_8 = c_{o,K^+}, \quad e_7 = e_8 - e_6, \quad e_5 = e_4 = e_6 = e_9$$

$$\dot{q}_5 = f_5 = f_4 + f_6 + f_9, \quad e_5 = \frac{1}{C}\int f_5 dt \quad = \frac{1}{C} q_5 = \frac{q_5}{C_m / q_e}$$

$$e_{10} = e_1 - e_{11},$$

$$f_{10} = f_1 = f_{11}, \quad f_{10} = \frac{e_{10}}{R_{Ca^{2+}}}$$

$$f_{12} = \frac{f_{11}}{q_e \cdot N_a}, \quad f_{17} = \dot{m}_{p,Ca^{2+}}, \quad f_{15} = \frac{e_{15}}{R'_{K^+}} = f_{14} = f_{16}$$

$$e_{16} = c_{o,K^+}, \quad e_{15} = e_{16} - e_{14}, \quad e_{13} = e_{12} = e_{14} = e_{17}$$

$$\dot{q}_{13} = f_{13} = f_{12} + f_{14} + f_{17}, \quad e_{13} = \frac{1}{C}\int f_{13}dt = \frac{1}{C}q_{13} = \frac{q_{13}}{C_m / q_e}$$

Substitution of variables between these equation groups will yield two equations for q_5 and q_{13}, which describe the charge contributions by the K^+ and the Ca^{2+} activities, respectively. An equation can be similarly obtained for Na^+.

3.1.2 State Equations for Ionic Dynamics

Based on Figures 3.3 and 3.4 and by following the procedure shown in the last subsection, six first-order equations can be derived for the Na^+, K^+ and Ca^{2+} ion concentrations in the outer segment and the inner compartment as summarized below. In each equation, the terms associated with membrane potentials (V_m^1, V_m^2) and electrical resistances (R_S) describe the ion fluxes driven by electric field, and the terms associated with concentrations (x_i) and material resistances (R'_S) compute the ion fluxes driven by diffusion.

$$z_{Na^+}FV_{cyto}^1 \cdot \frac{dx_1}{dt} = -\frac{V_m^1}{R_{cG,Na^+}} + \frac{[Na^+]_e - x_1}{R'_{cG,Na+}} + \dot{m}_{exchanger}(Na^+) + \frac{V_m^2 - V_m^1}{R_{thr,Na^+}} + \frac{x_2 - x_1}{R'_{thr,Na^+}} \qquad (3.1)$$

$$z_{Na^+}FV_{cyto}^2 \cdot \frac{dx_2}{dt} = -\frac{V_m^2}{R_{HCN_x,Na^+}} + \frac{[Na^+]_e - x_1}{R'_{HCN_x,Na+}} + \dot{m}_{pump}(Na^+) - \frac{V_m^2 - V_m^1}{R_{thr,Na^+}} - \frac{x_2 - x_1}{R'_{thr,Na^+}} \qquad (3.2)$$

$$z_{K^+}FV_{cyto}^1 \cdot \frac{dx_3}{dt} = \dot{m}_{exchanger}(K^+) + \frac{V_m^2 - V_m^1}{R_{thr,K^+}} + \frac{x_4 - x_3}{R'_{thr,K^+}} \qquad (3.3)$$

$$z_{K^+}FV_{cyto}^2 \cdot \frac{dx_4}{dt} = -V_m^2 \cdot \left(\frac{1}{R_{K_x}} + \frac{1}{R_{HCN_x,K^+}} + \frac{1}{R_{K(Ca)}}\right) + ([K^+]_e - x_4) \cdot \left(\frac{1}{R'_{K_x}} + \frac{1}{R'_{HCN_x,K^+}} + \frac{1}{R'_{K(Ca)}}\right)$$

$$+ \dot{m}_{pump}(K^+) - \frac{V_m^2 - V_m^1}{R_{thr,K^+}} - \frac{x_4 - x_3}{R'_{thr,K^+}} \qquad (3.4)$$

$$z_{Ca^{2+}} F V_{cyto}^{1} \cdot \frac{dx_5}{dt} = -\frac{V_m^1}{R_{cG,Ca^{2+}}} + \frac{[Ca^{2+}]_e - x_5}{R'_{cG,Ca^{2+}}} + \dot{m}_{exchanger}(Ca^{2+}) + \frac{V_m^2 - V_m^1}{R_{thr,Ca^{2+}}} + \frac{x_6 - x_5}{R'_{thr,Ca^{2+}}} \quad (3.5)$$

$$z_{Ca^{2+}} F V_{cyto}^{2} \cdot \frac{dx_6}{dt} = -\frac{V_m^2}{R_{Ca}} + \frac{[Ca^{2+}]_e - x_6}{R'_{Ca}} - \frac{V_m^2 - V_m^1}{R_{thr,Ca^{2+}}} - \frac{x_6 - x_5}{R'_{thr,Ca^{2+}}} \quad (3.6)$$

where

$$x_1 = [Na^+]_i^1, \quad x_2 = [Na^+]_i^2, \quad x_3 = [K^+]_i^1,$$

$$x_4 = [K^+]_i^2, \quad x_5 = [Ca^{2+}]_i^1, \quad x_6 = [Ca^{2+}]_i^2$$

z_S is the valence of ion *S*, where *S* represents Na^+, K^+ or Ca^{2+}. F is Faraday's constant. V_{cyto}^{j} Stands for the cytoplasmic volume of chamber *j*, where chamber *j* represents either the outer segment (when *j=1*) or inner compartment (when *j=2*).

The symbols, $\dot{m}_{exchanger}(Na^+)$, $\dot{m}_{exchanger}(K^+)$, $\dot{m}_{exchanger}(Ca^{2+})$, $\dot{m}_{pump}(Na^+)$, and $\dot{m}_{pump}(K^+)$, stand for the flux rates through Na/Ca-K exchangers and Na/K pumps in the photoreceptor membrane.

Based on the mechanisms of the exchanger and the pump (Kim, Reid et al. 1998), the corresponding flux rates for each ion species follow the relationships that

$$\dot{m}_{exchanger}(Na^+) : \dot{m}_{exchanger}(K^+) : \dot{m}_{exchanger}(Ca^{2+}) = 4:1:1 \quad (3.7)$$

$$\dot{m}_{pump}(Na^+) : \dot{m}_{pump}(K^+) = 3:2 \quad (3.8)$$

In following sessions for steady-state analysis, these flux rates are solved for and the specific values are

$$\dot{m}_{exchanger}(Na^+) = +5\,pA, \quad \dot{m}_{exchanger}(K^+) = -1.25\,pA, \quad \dot{m}_{exchanger}(Ca^{2+}) = -2.5\,pA,$$

$\dot{m}_{pump}(Na^+) = -23pA$, $\dot{m}_{pump}(K^+) = +15.33pA$;

3.1.3 Relation between R and R'

The method employed in obtaining the relationship between electrical resistance (R_r) and material resistance (R_r') is related to the procedure of deriving the Nernst-Planck eletrodiffusion equation. Before discussing their relationship, some of the notations needed in this section are listed. If the diffusing ion species is *S*, we use the following:

$z_S(dimensionless)$	Valence of ion *S*
$c_S(mol/cm^3)$	Local concentration of ion *S*
$M_S(mole/cm^2 \cdot s)$	Molar flux density of ion *S* (flux per unit area)
$M_{S,conc}(mole/cm^2 \cdot s)$	Molar flux density of ion *S* (flux per unit area) driven by concentration gradient
$M_{S,elec}(mole/cm^2 \cdot s)$	Molar flux density of ion *S* (flux per unit area) driven by electric field
$D_S(cm^2/s)$	Diffusion coefficient of ion *S*
$\mu_S[(cm/s)/(V/cm)]$	Mobility of ion *S* in membrane
$f_S[dyne/(cm/s)]$	Molecular frictional coefficient
$\psi(V)$	Local potential in membrane
$\triangle\psi(V)$	Membrane potential difference
$I_S(A/cm^2)$	Current density carried by ion *S* (per unit area)

$I_{S,conc}(A/cm^2)$	Current density carried by ion *S* (per unit area) driven by concentration gradient
$I_{S,elec}(A/cm^2)$	Current density carried by ion *S* (per unit area) driven by electric field
$A(cm^2)$	Permeation area

Fick's first law of diffusion relates aqueous diffusion flux to the product of the concentration field gradient and diffusion coefficient of the diffusing species S, i.e.

$$M_{S,conc} = -D_S \frac{dc_S}{dx} \tag{3.9}$$

which applies to the situation in absence of an electric field.

When there are no concentration gradients but only an electric field, the molar flux density of the aqueous diffusion flux is proportional to the strength of electric field, i.e.

$$M_{S,elec} = -z_S \mu_S c_S \frac{d\psi}{dx} \tag{3.10}$$

The current density is given by multiplying molar flux density with ionic valence and Faraday's constant.

$$I_{S,conc} = z_S F M_{S,conc} = -z_S F D_S \frac{dc_S}{dx} \tag{3.11}$$

$$I_{S,elec} = z_S F M_{S,elec} = z_S{}^2 F \mu_S c_S \frac{d\psi}{dx} \tag{3.12}$$

The Nernst-Einstein relationship between μ_S and D_S, obtained by using Eqns 3.9 and 3.10, is

$$D_S = \frac{kT}{f_S} = \frac{RT}{F} \mu_S \tag{3.13}$$

In Equation 3.11, $k \doteq 1.38065 \times 10^{-23} JK^{-1}$ is the Boltzmann constant that relates energy at particle level with temperature observed at bulk level. T represents absolute temperature in Kelvin. $R = 8.31447 JK^{-1}mol^{-1}$ is the universal gas constant.

Combining Equations 3.9, 3.10 and 3.11, gives the Nernst-Planck eletrodiffusion equation:

$$I_S = z_S F D_S \left(\frac{dc_S}{dx} + \frac{F z_S c_S}{RT} \frac{d\psi}{dx}\right) \tag{3.14}$$

When an ionic flux is going through ion channels in a cell membrane, the channels may have various influences on the flux, such as: (1) eletrostatic repulsion by other ions in the channel pole, (2) mechanical interactions with ion molecules of other species or water molecules. β is used as a factor to account for these effects. It is reasonable to assume that the channel effect influences the ionic diffusion flux and the electric-field driven flux in the same manner.

Including the channel effect β in Eqns 3.9 and 3.10, the diffusion fluxes through ion channels driven either by concentration gradient or by electric field become

$$M_{S,conc} = -D_S \beta \frac{dc_S}{dx} \tag{3.15}$$

$$M_{S,elec} = -z_S \mu_S c_S \beta \frac{d\psi}{dx} \tag{3.16}$$

and the new current density would be

$$I_{S,conc} = z_S F \beta M_{S,conc} = -z_S F \beta D_S \frac{dc_S}{dx} \tag{3.17}$$

$$I_{S,elec} = z_S F \beta M_{S,elec} = z_S{}^2 F \beta \mu_S c_S \frac{d\psi}{dx} \tag{3.18}$$

Combining Equations 3.15, 3.16 and 3.17, gives the Nernst-Planck eletrodiffusion

equation with channel effect β included:

$$I_S = z_S F \beta D_S \left(\frac{dc_S}{dx} + \frac{F z_S c_S}{RT} \frac{d\psi}{dx}\right) \tag{3.19}$$

For the ionic diffusion flux driven by concentration gradient, if we take dc_S / dx (or $\triangle c_S$) as the driving force, the diffusion resistance, R_r', can be defined by the following relationship:

$$I_{S,conc} = -\frac{1}{A} \frac{1}{R_r'} \frac{dc_S}{dx} \tag{3.20}$$

For flux between two points, if the concentration changes linearly, the above relation can be re-defined as

$$I_{S,conc} = -\frac{1}{A} \frac{\triangle c_S}{R_r'} \tag{3.21}$$

Together with Eqn 3.15, Eqn 3.21 gives

$$I_{S,conc} = -\frac{1}{A} \frac{\triangle c_S}{R_r'} = -z_S F \beta D_S \frac{\triangle c_S}{\triangle x} \tag{3.22}$$

As a result,

$$R_r' = \frac{\triangle x}{z_S F \beta D_S A} \tag{3.23}$$

For ionic diffusion flux driven by electric field, applying Ohm's law, gives

$$I_{S,elec} = -z_S{}^2 F \beta \mu_S c_S \frac{d\psi}{dx} = -\frac{1}{A} \frac{1}{R_r} \frac{d\psi}{dx}$$

Similarly, when concentration changes between two points follow a linear relationship, above equation can be re-defined as

$$I_{S,elec} = -z_S{}^2 F \beta \mu_S c_S \frac{\triangle \psi}{\triangle x} = -\frac{1}{A}\frac{\triangle \psi}{R_r}$$

i.e.
$$R_r = \frac{\triangle x}{z_S{}^2 F \beta \mu_S c_S A} \tag{3.24}$$

From Equations 3.23 and 3.24, the relationship between R_r and R_r' is

$$\frac{R_r'}{R_r} = \left(\frac{\triangle x}{z_S F \beta D_S A}\right) / \left(\frac{\triangle x}{z_S{}^2 F \beta \mu_S c_S A}\right) = \frac{z_S \mu_S c_S}{D_S} \tag{3.25}$$

With the Nernst-Einstein relationship (Eqn 3.19), Eqn 3.25 can be simplified as

$$\frac{R_r'}{R_r} = z_S c_S \frac{\mu_S}{D_S} = z_S c_S \frac{F}{RT}$$

i.e.
$$\frac{R_r'}{R_r} = \frac{z_S F}{RT} \cdot c_S \tag{3.26}$$

For a given ion species *S*, assume the resistance values at two different concentrations levels of c_1 and c_2 are $R_{r,1}$ and $R_{r,2}$ respectively, we have

$$R_{r,1} \cdot c_1 = \frac{\triangle x}{z_S{}^2 F \mu_S A} = R_{r,2} \cdot c_2 \tag{3.27}$$

which shows that the product of concentration and electric resistance would be a constant, provided that the assumption of same channel effects holds.

3.1.4 Computation of Membrane Voltage V_m

What is well known for computing the cell membrane voltage in cell membrane physiology is the Goldman-Hodgkin-Katz Equation, which models the resting membrane potential, or equilibrium membrane potential, in the presence of multiple ion species

permeable to the cell membrane. However, what we need here is a way to determine the cell membrane potential not only at equilibrium, but more importantly, in transient, i.e. when the cell is not at the resting state. The transient state of a cell depends on the physiological properties of the cell (such as size, shape, membrane structure and thickness), and the distribution of ions both intracellularly and extracellularly.

Most existing studies are performed in an opposite way, in which cells are voltage-clamped at fixed membrane potentials and tested for various intrinsic membrane electric properties. There have been studies with fluorescent dye which can respond to change in electric voltage levels. The intensity of fluoresence is taken as an indicator of the membrane voltage level. In other studies, the membrane voltage is recorded as a function of time, and computer programs are utilized to re-play the process of action potentials.

For estimating the electric potential across the cell membrane of a rod photoreceptor, we made the following assumptions:

1) The rod photoreceptor cell consists of two connected chambers of cylindrical shape.
2) Charges are evenly distributed outside of the cell. Excessive charges instantly diffuse away.

In the following, the outer segment is taken as an example for calculating the membrane potential, and the method remains the same when applied to the inner compartment. Concentrations inside and outside of the cell for ion species *S* are denoted by c_{in}^{S} and c_{ex}^{S} (or c_{in} and $_{\mathrm{S}}$ for general representation). The cell membrane has a thickness of $\triangle r$, and the

length and the radius of outer compartment are L and r, respectively.

1. By Gauss' law, the electric field generated by charges inside the cylinder can be described as

$$E_1 = \frac{1}{\varepsilon_0 \cdot 4\pi r^2} \sum_i (\frac{4}{3}\pi R^3) \cdot (c_{in} \cdot z_{in})_i \cdot F$$

$$= \frac{1}{3\varepsilon_0 r^2} \cdot R^3 \cdot \sum_i (c_{in} \cdot z_{in})_i \cdot q_e \cdot F \qquad (r \geq R + \triangle R)$$

2. As we assumed charges to be evenly distributed outside the cell, the electric field generated by outside charges should be of the opposite direction of the field generated by the inside area (with radius $R+\Delta R$) filled with the same charge concentration.

   Hence, from Gauss' law, the electric field generated by charges outside of the cylinder can be described as

$$E_2 = -\frac{1}{\varepsilon_0 \cdot 4\pi r^2} \sum_j \frac{4}{3}\pi (R + \triangle R)^3 \cdot (c_{out} \cdot z_{out})_j \cdot F$$

$$= -\frac{1}{3\varepsilon_0 r^2} (R + \triangle R)^3 \sum_j (c_{out} \cdot z_{out})_j \qquad (r \geq R + \triangle R)$$

3. The overall electric field generated would be

$$E = E_1 + E_2$$

$$= \frac{1}{3\varepsilon_0 r^2} \cdot F \cdot [R^3 \cdot \sum_i (c_{in} \cdot z_{in})_i - (R + \triangle R)^3 \cdot \sum_j (c_{out} \cdot z_{out})_j]$$

$$= \frac{R^3}{3\varepsilon_0 r^2} \cdot F \cdot [\sum_i (c_{in} \cdot z_{in})_i - (1 + \triangle R / R)^3 \cdot \sum_j (c_{out} \cdot z_{out})_j] \qquad (r \geq R + \triangle R)$$

At $r = R + \triangle R$,

$$E = \frac{R+\triangle R}{3\varepsilon_0} \cdot F \cdot [\frac{1}{(1+\triangle R/R)^3} \sum_i (c_{in} \cdot z_{in})_i - \sum_j (c_{out} \cdot z_{out})_j]$$

Therefore, across the membrane the integration of E is:

$$\begin{aligned} V_m &= \int_{-\infty}^{R} E dr - \int_{-\infty}^{R+\triangle R} E dr \\ &= \{-\frac{R^3}{3\varepsilon_0 r} \cdot F \cdot [\sum_i (c_{in} \cdot z_{in})_i - (1+\triangle R/R)^3 \sum_j (c_{out} \cdot z_{out})_j]\} |_{R+\triangle R}^{R} \\ &= -\frac{R^3}{3\varepsilon_0} (\frac{1}{R} - \frac{1}{R+\triangle R}) \cdot F \cdot [\sum_i (c_{in} \cdot z_{in})_i - (1+\triangle R/R)^3 \sum_j (c_{out} \cdot z_{out})_j] \end{aligned} \quad (3.28)$$

which is the membrane voltage. The direction of V_m is from outside to inside.

When there is only one charge species with valence z, we have the membrane potential as

$$E = \frac{zF}{3\varepsilon_0 r^2} \cdot [R^3 \cdot c_{in} - (R+\triangle R)^3 \cdot c_{out}]$$

$$= \frac{zF \cdot R^3}{3\varepsilon_0 r^2} \cdot [c_{in} - (1+\triangle R/R)^3 \cdot c_{out}]$$

And at $r = R+\triangle R$,

$$E = \frac{zF(R+\triangle R)}{3\varepsilon_0} \cdot [\frac{1}{(1+\triangle R/R)^3} \cdot c_{in} - c_{out}] \quad (3.29)$$

3.2 Steady State Analysis

An important verification of the state equations is that the equations should be capable of describing the steady state correctly. In particular, they should discribe the steady state where photoreceptors are placed in the dark. The analysis will also provide the resistance values consistent with the circulating current in its actual physiological condition.

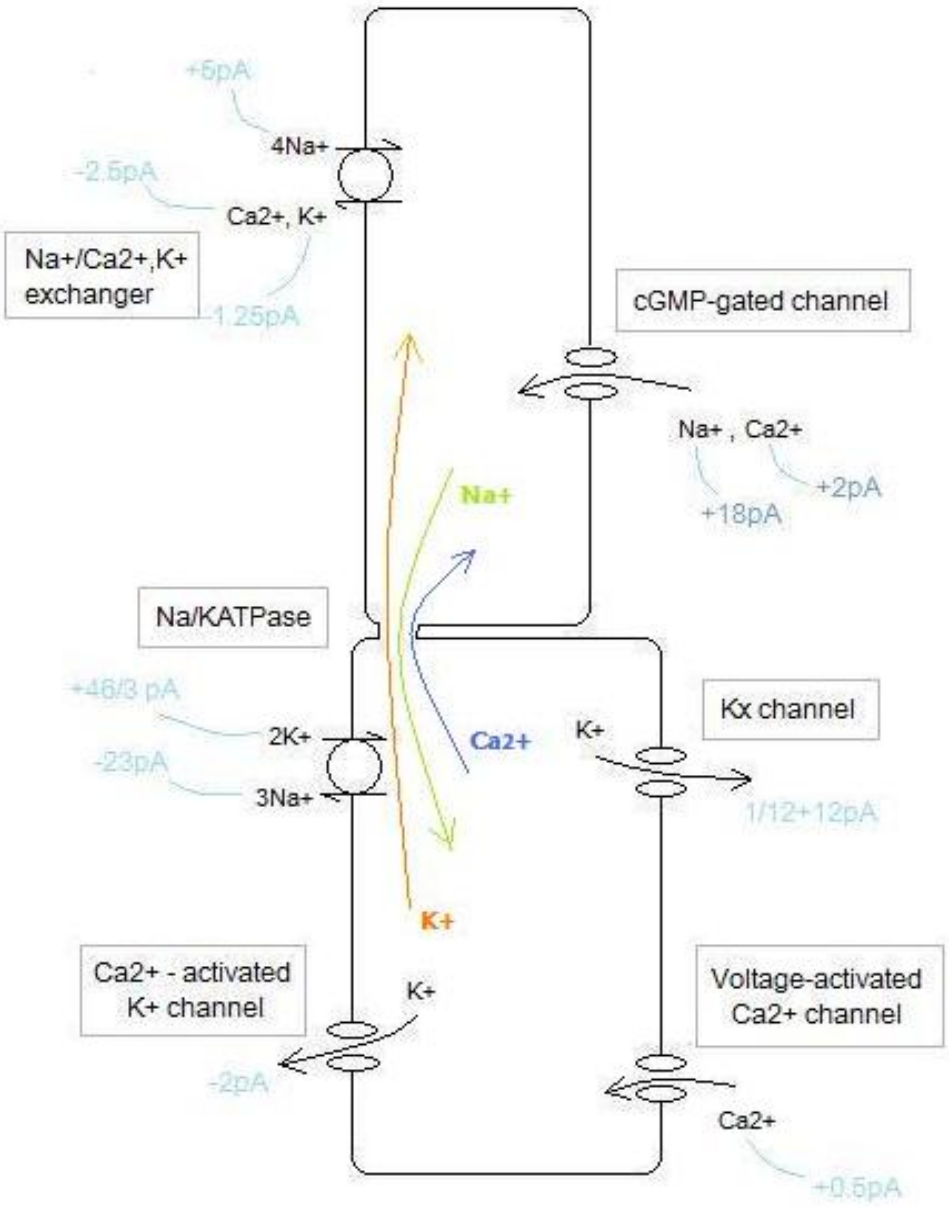

Figure 3.5 Schematic of ion channel activities of a rod cell placed in darkness.

The cGMP-gated channel in the outer segment is open and allows a constant influx of Na^+ and Ca^{2+} ions. As shown in existing literature, the current carried by this influx is around 20pA for mouse rods (Xu et al., 1997). Thereby, in this analysis the dark current is taken as 20pA.

In the inner compartment, the K_x channel, the voltage-activated Ca^{2+} channel and the Ca^{2+}-activated K^+ channel (K(Ca) channel) are also kept open. As mentioned in Chapter 2, the K(Ca) channels, instead of producing the major waveform of the photoresponse current, serve to provide further depolarization of the cell with influx of Ca^{2+} through voltage-activated Ca^{2+} channels and to repolarize the cell when the Ca^{2+} channels are closed. There are no reported exact data for the currents carried by these three types of channels; however, we may infer from the channel functions that the latter two are permeating relatively much smaller currents than the cGMP-gated channel and K_x channel. Hence, we assume a 0.5pA inward current for the voltage-activated Ca^{2+} channel, and a 2pA outgoing current for the Ca^{2+}-activated K^+ channel (K(Ca) channel), i.e.

$$I_{Ca} = +0.5\,pA$$
$$I_{K(Ca)} = -2\,pA$$

Where '-' sign indicates outward direction, '+' sign indicates inward direction.

With these estimations and the experimentally measured dark value for the cGMP-gated channel, we can determine the currents through the ion exchangers/pumps and the other channels. Furthermore, substituting the results into the state equations at steady state, a set of nonlinear constraints will be obtained, from which estimations can be obtained for the values of channel resistance, concentrations of ions inside the cell, and membrane potential at steady state.

There are three paths of Ca^{2+} to flow into or out of the cell: cGMP-gated channel,

voltage-activated Ca^{2+} channel, and Na/Ca-K exchanger. Since the net Ca^{2+} flux is zero at the steady state, i.e.

$$I_{CNG,Ca^{2+}} + I_{Ca} + \dot{m}_{exchanger}(Ca^{2+}) = 0$$

the Ca^{2+} exchanger flux should be opposite to the algebraic sum of the other two fluxes, which is

$$\dot{m}_{exchanger}(Ca^{2+}) = -(2\,pA + 0.5\,pA) = -2.5\,pA$$

Based on the mechanism of Na/Ca-K exchanger, in Eqn (3.7), the ratio among exchanged Na^+, Ca^{2+} and K^+ is 4:1:1 (Kim, Reid et al. 1998), we get

$$\dot{m}_{exchanger}(Na^+) = +5\,pA$$
$$\dot{m}_{exchanger}(K^+) = -1.25\,pA$$

These ionic current values determined for the the outer segment are marked in Figure 3.5.

In the three Na^+ currents, two of them are already estimated, which are the current through cGMP-gated channels (+5pA) and the current produced by the exchanger (+18pA). Thereby, the Na^+ current generated by the Na^+/K^+-ATPase needs to be

$$\dot{m}_{pump}(Na^+) = -(+5\,pA + 23\,pA) = -23\,pA,$$

at steady state. By the mechanism of the pump, the Na^+ flux should be 3/2 of K^+ flux as presented in Eqn (3.8), which gives

$$\dot{m}_{pump}(K^+) = +15\frac{1}{3}\,pA.$$

Now, if we take an algebraic sum of all the known K^+ currents, the K^+ current through K_x channels, which is the only one left undetermined, should be equal to the inverse of this sum,

that is

$$I_{K_x} = -(-1.25\,pA + 15\frac{1}{3}\,pA - 2\,pA) = -12\frac{1}{12}\,pA.$$

In Figure 3.5, these currents have also been marked. This allowed us to find the direction and magnitude of currents through the connecting cilium. To be specific, at the steady state, the Na^+ current is flowing down from the outer segment to the inner compartment, whereas K^+ and Ca^{2+} currents are moving from the inner compartment to the outer segment. These three currents would be 23pA, 1.25pA and 0.5pA, respectively.

By the symbols used for the state equations (Equations 3.1 - 3.6), the steady-state currents give the following set of steady-state equations:

$$+18\,pA = -\frac{V_m^1}{R_{cG,Na^+}} + \frac{[Na^+]_e - x_{1,SS}}{R'_{cG,Na+}} \tag{3.30}$$

$$-23\,pA = \frac{V_m^2 - V_m^1}{R_{thr,Na^+}} + \frac{x_{2,SS} - x_{1,SS}}{R'_{thr,Na^+}} \tag{3.31}$$

$$1.25\,pA = \frac{V_m^2 - V_m^1}{R_{thr,K^+}} + \frac{x_{4,SS} - x_{3,SS}}{R'_{thr,K^+}} \tag{3.32}$$

$$-12\frac{1}{12}\,pA = -\frac{V_m^2}{R_{K_x}} + \frac{([K^+]_e - x_{4,SS})}{R'_{K_x}} \tag{3.33}$$

$$-2\,pA = -\frac{V_m^2}{R_{K(Ca)}} + \frac{[K^+]_e - x_{4,SS}}{R'_{K(Ca)}} \tag{3.34}$$

$$0.5\,pA = \frac{V_m^2 - V_m^1}{R_{thr,Ca^{2+}}} + \frac{x_{6,SS} - x_{5,SS}}{R'_{thr,Ca^{2+}}} \tag{3.35}$$

$$+2\,pA = -\frac{V_m^1}{R_{cG,Ca^{2+}}} + \frac{[Ca^{2+}]_e - x_{5,SS}}{R'_{cG,Ca^{2+}}} \tag{3.36}$$

$$+0.5pA = -\frac{V_m^2}{R_{Ca}} + \frac{[Ca^{2+}]_e - x_{6,SS}}{R'_{Ca}} \tag{3.37}$$

In the next section, a steady-state analysis will be shown based on the above equations, which will give equilibrium resistance values to be used as the starting point for transient response analysis.

3.3 Steady State Solution

Based on the analysis in the previous section, the steady-state equations can be solved for the channel resistance values that are unknown at this point.

Ionic concentration values under normal physiological conditions for rod photoreceptor cells are used (Table 3.1).

Steady-State parameters	Na^+ (mM)	K^+ (mM)	Ca^{2+} (nM)	V_m (mV)	V_{cyto} (μm^3)
Outer segment	5	159.2328562	320	-37	19
Inner compartment	5.402181364	172.1	450	-39	20
Extracellular	145	4	1	0	-

Table 3.1 Concentration values for rod photoreceptors under normal physiological conditions.

The resting membrane potential is adjusted to be at -37 mV and -39 mV for the outer segment and the inner compartment, respectively, which is within the normal range of the membrane potential for a rod photoreceptor cell (Kraft et al., 1993; Schneeweis and Schnapf,

1995). During receptor responses and at the resting state, the general relationship between membrane potential V_m and ion distributions follows the form derived in section 3.1.4 (in Eqns (3.22) and (3.23)) in which V_m is linearly proportional to the net charge density difference between extracellular and intracellular environments. The specific relations applied in the model are as follows:

$$V_m^1 = \left([Na^+]_i^1 + [K^+]_i^1 + [Ca^{2+}]_i^1 * 2 - [Na^+]_e - [K^+]_e - [Ca^{2+}]_e * 2 - A\right) * K_1 + V_{m,SS}^1$$
$$V_m^1 = \left([Na^+]_i^2 + [K^+]_i^2 + [Ca^{2+}]_i^2 * 2 - [Na^+]_e - [K^+]_e - [Ca^{2+}]_e * 2 - B\right) * K_2 + V_{m,SS}^2$$

where

$$A = \left[x_{10} + x_{12} + x_{14} * z_{Ca^{2+}} - [Na^+]_e - [K^+]_e - [Ca^{2+}]_e * z_{Ca^{2+}} \right]$$
$$B = \left[x_{11} + x_{13} + x_{15} * z_{Ca^{2+}} - [Na^+]_e - [K^+]_e - [Ca^{2+}]_e * z_{Ca^{2+}} \right]$$

The ratio K_1 and K_2 are constant parameters, and were set as equal to 2.29125 and 2.291, respectively.

The concentration values employed in the steady-state may not be the same as actual values in rods, but they are the best estimates from published literature. Changes in the choices of these values can be easily made in the model and to give a new solution. This is also one of the advantages offered by this modeling approach.

For the given concentration levels, the resistance values that satisfy the steady-state equations are solved for and summarized in Table 3.2.

Ionic conductance		CNG channel	Connecting Cilium	K_x channel	HCH_x channel	K(Ca) channel	Voltage-gated Ca channel
Na^+	*R*	5.06E+11	1.99E+06	0	6.68E+11	0	0
	R'	1.89E+13	7.45E+07	0	2.50E+13	0	0
K^+	*R*	0	1.35E+06	2.17E+12	2.00E+12	3.59E+11	0
	R'	0	5.06E+07	8.11E+13	7.49E+13	1.34E+13	0
Ca^{2+}	*R*	5.04E+10	3.36E+06	0	0	0	2.09E+11
	R'	1.88E+12	1.25E+08	0	0	0	7.83E+12

Table 3.2. Resistance values satisfying the steady-state equations.

3.4 A Normal Photoreceptor Response to Light Stimulus

When provided light stimulus, the cGMP-gated channels begin to close, leading to a series of channel closing and activating activities that shape a photoreceptor light response. As mentioned in Chapter 2, dim flashes can induce receptor responses of small amplitudes, whereas strong light pulses are able to elicit larger responses that may involve the hyperpolarization-activated channels (I_h channels).

In the model, the closing ratio of cGMP-gated channel is used as a trigger for the whole receptor response. The channel kinetics of each channel types is implemented in the model based on the related experimental data and the activation curves of the channel as illustrated in Chapter 2. The photoreceptor response to light is modeled as proportional to the changes

in the circulating current. Figure 3.6 illustrates a simulation curve of photoreceptor response normalized to 1. The channel closing ratio of cGMP-gated channel is equal to 95% mimicing the experimental condition of strong light stimulus.

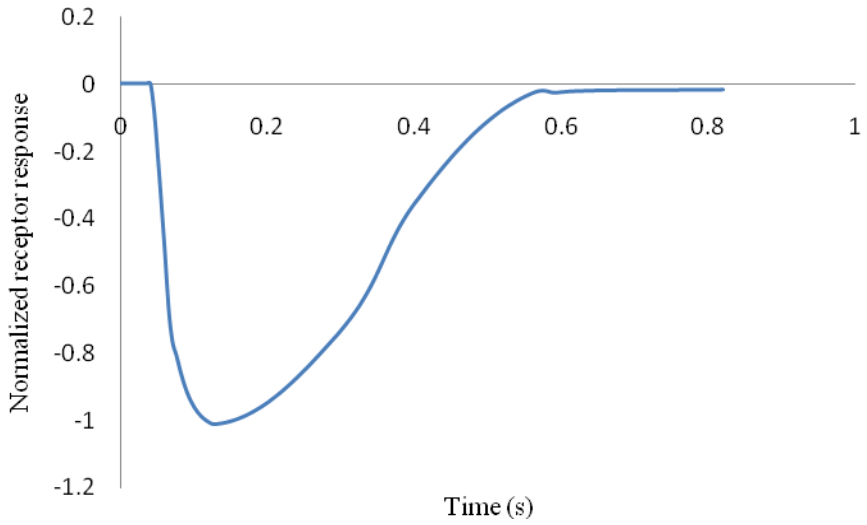

Figure 3.6 Standard receptor response curve from model simulating response to strong light flash. The response is normalized to 1. Light pulse is administrated at time t = 0.062 s.

The response lasts for roughly 0.6 sec. Within the response, the phototransduction cascade-induced initial drop lasts for ~110 ms. This is in agreement with previous observations that dim-flash responses reach peak in around 200 ms (at mammlian body temperature) whereas responses elicited by bright flashes reach peak earlier (Pugh and Lamb, 2000).

Ionic related activities inside a photoreceptor cell are also obtained and recorded through simulation. Figure 3.7 presents the simulation curves for these activities, including concentration changes of major ion species (Na^+, K^+ and Ca^{2+}) and membrane voltages

(V_m^1, V_m^2) of the outer segment and inner compartment.

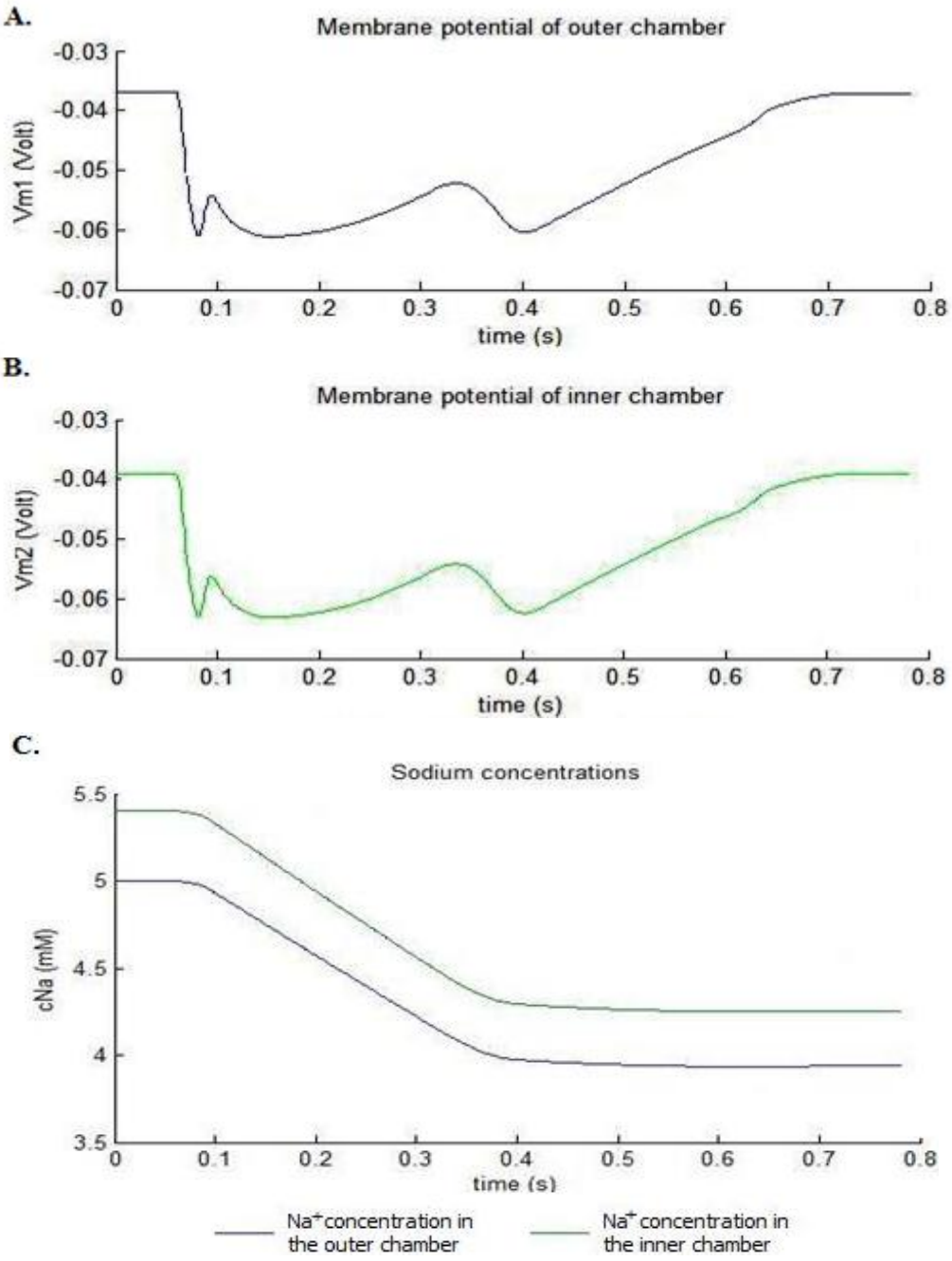

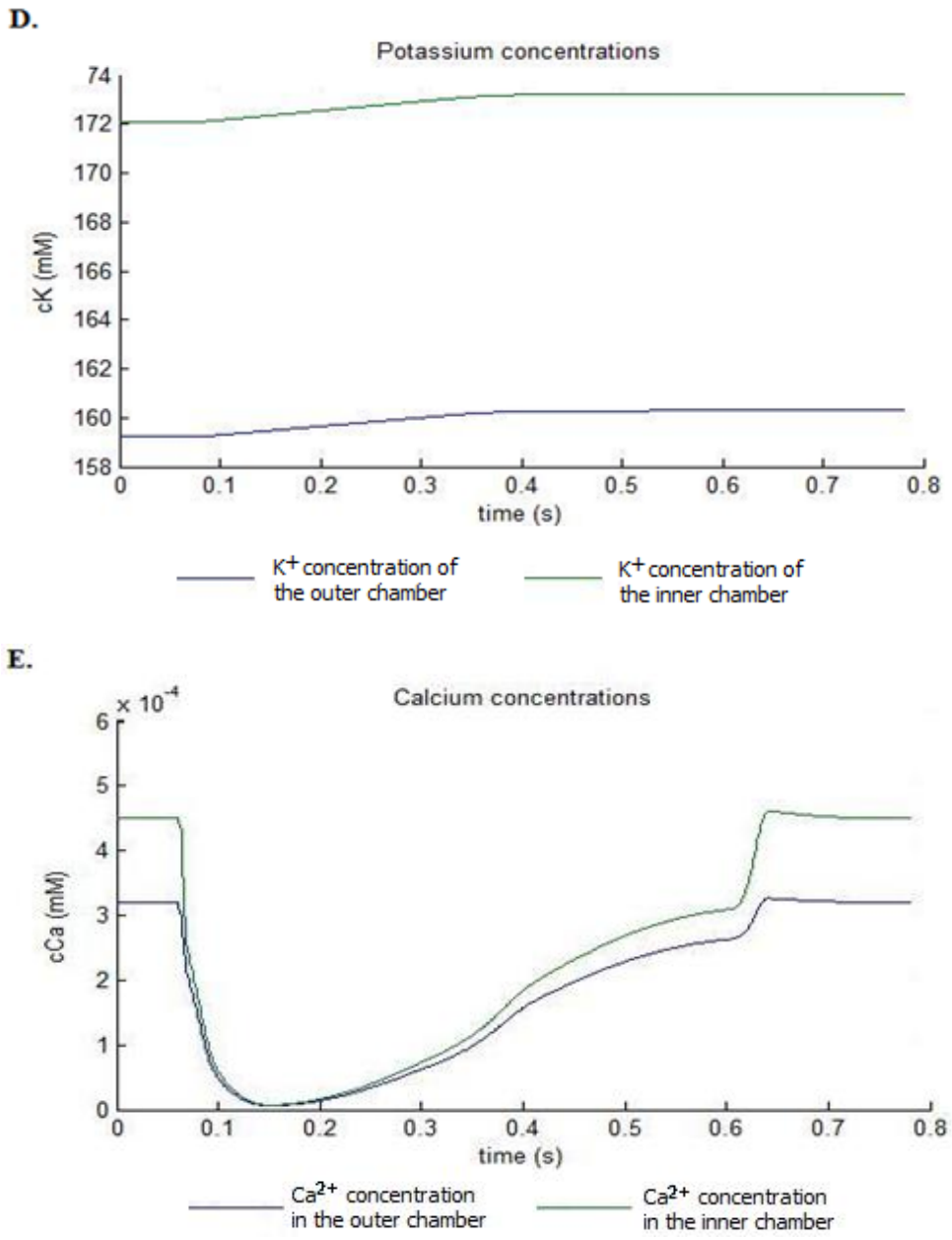

Figure 3.7. Simulation curves for ionic activities during photoreceptor response to strong light flash, including concentrations changes of Na^+(B), K^+ (C), and Ca^{2+}(D), and membrane voltages (V_m^1, V_m^2) of the outer segment (A) and the inner compartment (B).

In the next chapter, we will present simulation results from the model for different conditions or disease stages.

CHAPTER 4

MODEL VALIDATION

The model for rod photoreceptor cell light response derived in the previous chapter is applied to several experimental conditions and validated with experimental data. Specifically, receptor responses induced by light stimuli of different intensities were simulated, and degenerations of different parts of the transport process in rod photoreceptor were tested and simulated to compare with actual experiment data.

4.1 Receptor Response under Different Light Flash Intensities

In this section, simulation results from the model are present for receptor responses to different light intensities. Data from Kang Derwent et al (2006) for bright flash ERG experiments are used to validate the model.

In a study conducted by Kang Derwent et al (2006), normal cats and eight Abyssinian cats with hereditary retinal degeneration were studied with bright-flash ERG recordings. Bright flashes were used to induce strong ERG waves so that the initial phase of the ERG (a-waves) would be robust and not covered by the b-waves.

Figure 4.1 illustrates the ERG of a normal, dark-adapted cat retina in response to bright, brief stimuli. The flash intensity ranged from 2.93 to 7.93 log photoisomerizations per rod per flash. Original recordings (A) and normalized responses (B) are provided.

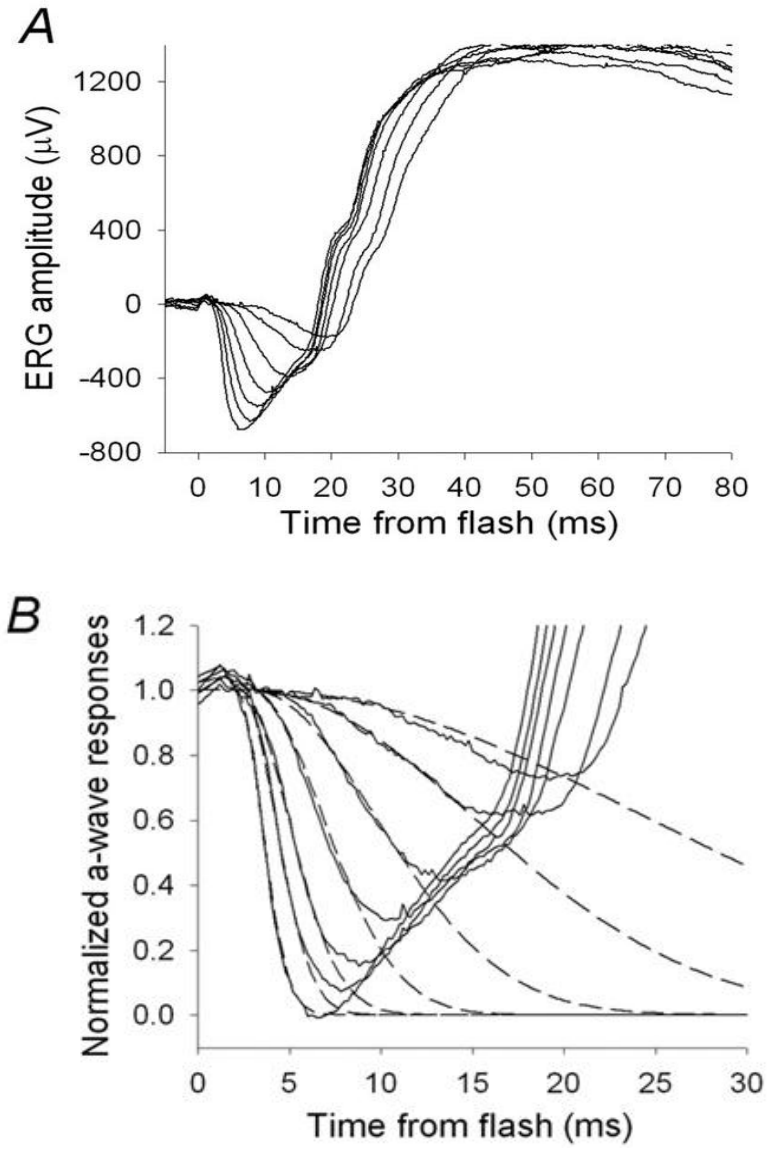

Figure 4.1 ERG of a normal, dark-adapted cat retina in response to bright, brief stimuli. The flash intensity varied from Φ = 2.93 to 7.93. Original recordings (A) and normalized a-wave responses of figure (A) to saturated a-wave amplitude (B). (Kang Derwent et al, 2006)

Figure 4.1 shows that with increased light flash intensity, the amplitude of a-wave grows larger. However, due to the strong initiation of b-wave, the time-to-peak for a-wave cannot be exactly obtained. Still, a shift in initiation time point for b-wave can be observed and the initiation time prolongs as light intensity gets weaker.

Some possible explanations we would propose for this are: (1) stronger light flash stimuli induces a more rapid receptor response that has a smaller time constant; (2) since b-wave, elicited primarily by the bipolar cells, depends on the accumulation of the neurotransmitter released from the photoreceptor synaptic terminal, smaller light flash intensity would result in smaller photoreceptor response that induces a smaller velocity of neurotransmitter release, hence a longer time frame for b-wave to initiate and the point of initiation appears to shift to right; and (3) a combination of (1) and (2) is also highly likely, in other words, there might be an actual shift for peak photoreceptor response as given by (1), but (2) also plays a significant role in the shift of b-wave initiation.

Flashes applied to rod photoreceptors lead to closure of cGMP-gated channels in the outer segment, which, in the model, serves as the trigger to receptor responses. Therefore, model simulation of receptor responses is achieved by changing the cGMP-channel closing ratio.

Figure 4.2 shows the simulation curves of bright-flash responses. The response amplitude increases as the closing ratio of cGMP-gated channels increases in response to elevated light flash intensity. A shift of peak response that points to the left can be noticed with varied flash intensity but is not very significant, which coincides with the experiment data provided by Kang Derwent et al (2006).

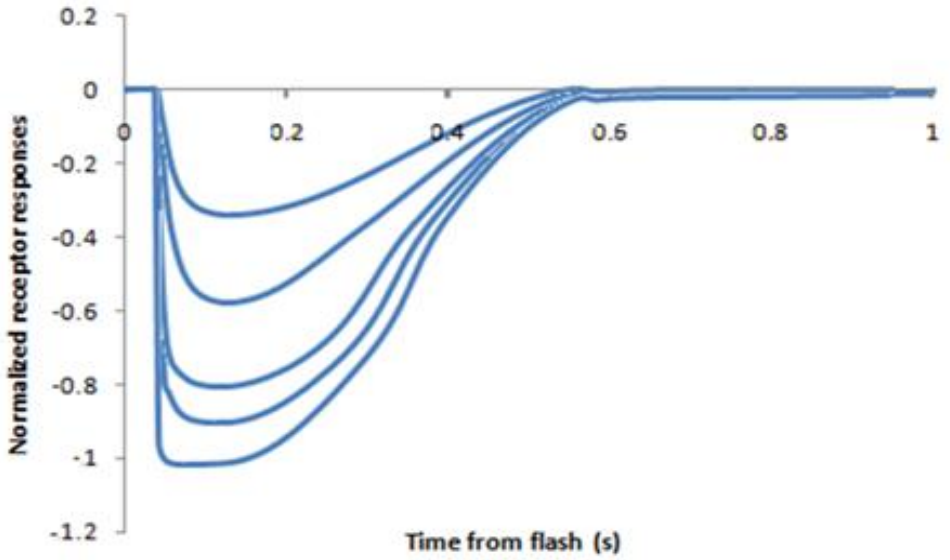

Figure 4.2 Simulation of the photoreceptor responses to bright flashes of different light intensities. The responses are normalized to -1.

4.2 Receptor Response with Abnormality in the Rod Connecting Cilium (CC)

Abyssinian cats affected with a hereditary retinal degeneration disease, first discovered in 1985 (Narfstrom 1985), has similarities to human retinitis pigmentosa (RP). In the diseased stages, observed degeneration in vision can be reflected in the changes of ERG recordings. It has been confirmed that rod photoreceptor dysfunction plays a bigger role in the ERG changes compared to the loss of rods (Kang Derwent et al., 2006). Recently the gene responsible for this disease was identified, and found to have a major influence on the rod connecting cilium (Narfstrom, 1983; Pazour et al., 2002; Badano et al., 2006). Therefore, modeling how changes in connecting cilium structure and transport may affect the receptor responses produced by rod photoreceptors can be important for understanding and elucidation of disease mechanisms.

Since the connecting cilium links the outer segment and the inner compartment, a small change in it may have a significant influence on the function of the whole cell. This includes possible influence on the exchange of ionic fluxes and protein transport between outer segment and inner compartment.

In the following sections, influences caused by reduction in CC ion transport on the dark resting state and the receptor responses related to age and disease stage are simulated and presented.

4.2.1 Changes in Dark Resting State with Reduction in Ion Transport Through the Connecting Cilum

With changes in connecting cilium ion transport, the dark resting state of the rod photoreceptor is also reset. Changes include resetting of ion concentrations for all species in both outer segment and inner compartment, suppression of the dark circulating current, and membrane voltages for the two segments. We simulated the changes in the ionic fluxes and distribution of ions in the outer segment and inner compartment that may result from changes in the connecting cilium.

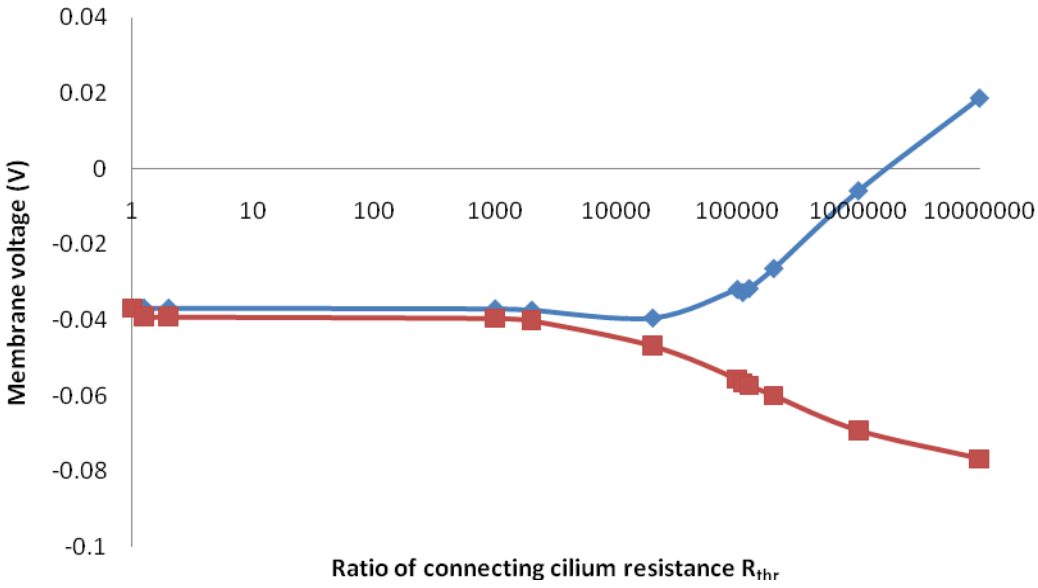

Figure 4.3 Membrane voltages for outer segment (blue diamonds) and inner (red squares) compartment, as a function ion transport resistance of the connecting cilium.

Figure 4.3 shows the steady-state membrane voltage for outer segment and inner compartment in response to changes in ion transport resistance through the connecting cilium. It can be observed that, with an increase in connecting cilium resistance, the outer segment becomes more depolarized, while membrane voltage for the inner compartment goes to the opposite direction that makes the inner compartment more hyperpolarized. Changes in V_m do not become significant until the connecting cilium resistance is increased by a factor of 1000.

Similar changes were also observed for ion concentrations of K^+, Na^+ and Ca^{2+} in two segments. Whereas K^+ and Na^+ concentrations still stay within the normal physiological ranges, changes in the Ca^{2+} ion concentration is worth consideration. When the connecting cilium resistance increases, the resting Ca^{2+} concentrations in both segments are raised to a

high level. Compared with the normal Ca^{2+} concentration in rod (~100nM - 400nM), Ca^{2+} concentration can rise to ~ 0.6μM, which is more than 10 times of normal value. Since Ca^{2+} ion is very import for cell activity, it may be important to study the effect of elevated Ca^{2+} on cell function.

Figure 4.4 shows the dark circulating current versus reduction ratio of CC conductance.

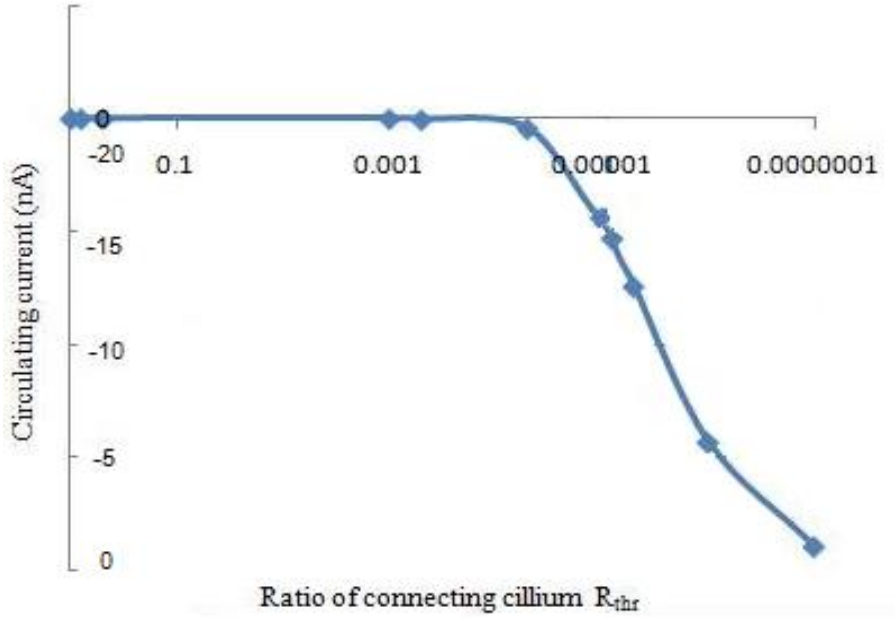

Figure 4.4 Circulating current for different reduction in conductance of the connecting cilium.

Figure 4.4 shows that the conductance decrease in the connecting cilium causes the dark circulating current to be reduced. However, suppression of the circulating current is not significant until the connecting cilium conductance is reduced by a factor of 1000.

4.2.2.1 Rod Photoreceptor Response with Reduction in Ion Transport through CC

In this section, the model is applied to analyze how a reduction in connecting cilium

conductance may affect the photoreceptor response to light.

Figure 4.6 shows the reduction of peak receptor response versus the reduction in conductance and thus, in ionic transport through the connecting cilium. With a greater reduction in connecting cilium, the corresponding peak receptor response becomes more suppressed as shown in both Figures 4.5 and 4.6.

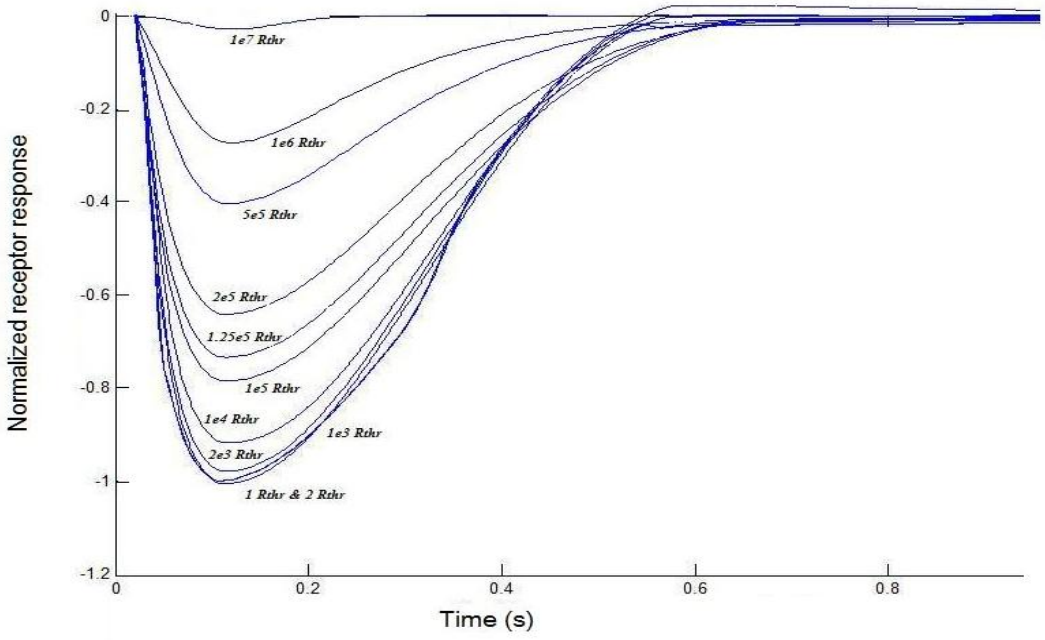

Figure 4.5 Simulation of receptor response with connecting cilium conductance as a parameter. The responses are normalized to -1 with respect to receptor response of a normal rod photoreceptor.

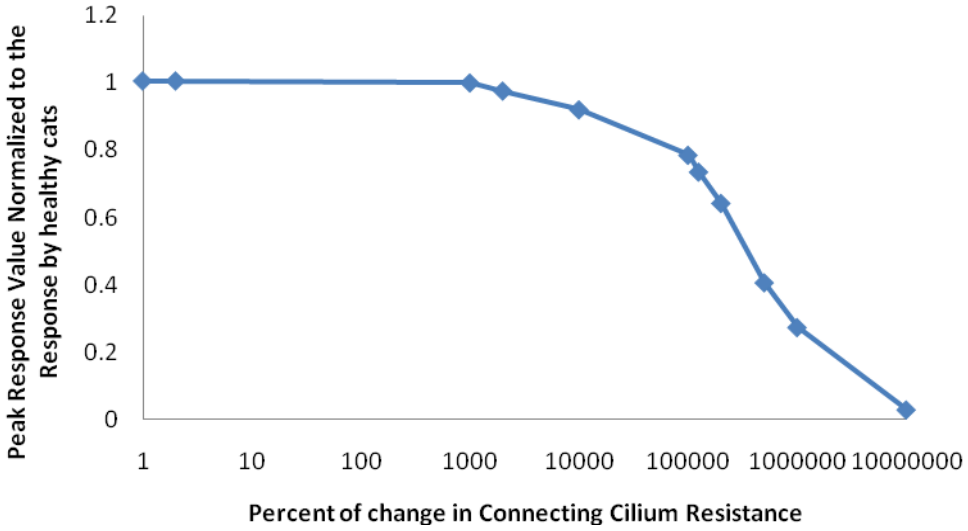

Figure 4.6 Model simulation of reduction of peak receptor response cause by the reduction in ionic transport through the connecting cilium. The responses are normalized to 1 with respect to receptor response of a normal rod photoreceptor.

4.2.2.2 Age-related Receptor Degeneration in Ion Transport through the Connecting Cilium

Figure 4.7 shows a model simulation of the reduction of peak receptor response versus the reduction in ionic transport through connecting cilium. With narrowing in the connecting cilium, the corresponding peak receptor response becomes more suppressed.

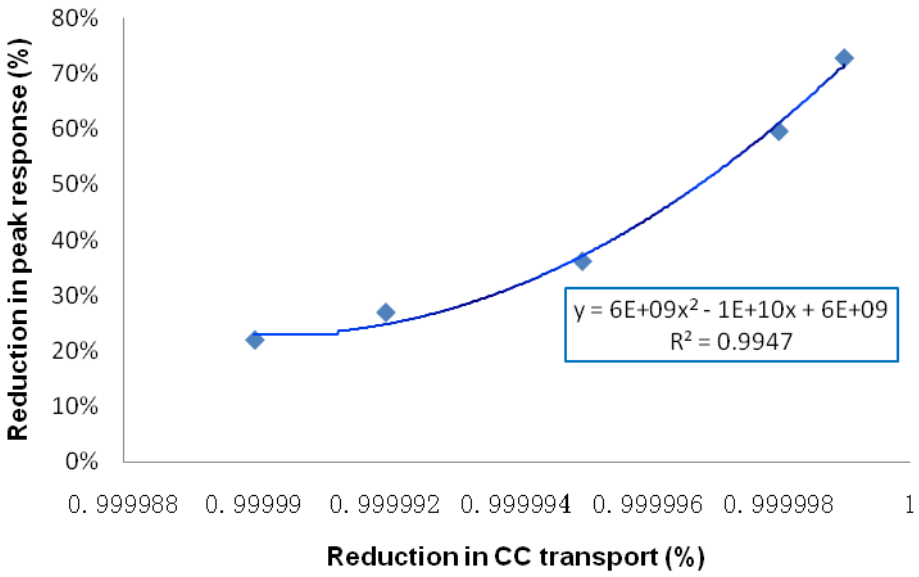

Figure 4.7 Model simulation of the percentage of reduction in peak receptor response cause by the reduction in ionic transport through the connecting cilium, relative to the response of a normal rod.

Table 4.1 summarizes an ERG study on 97 cats over a 7-year period by a group lead by Dr. Kristina Narfström. High intensity-stimulation was given to dark-adapted normal and affected cats of all age groups, and both a-wave and b-wave amplitudes were recorded. With increasing age, the disease progresses, with reductions in both a- and b-waves of ERG.

Age group (months)	Mean amplitude decrease		Approximate funduscopic stage of disease
	a-wave	b-wave	
13 - 15.5	28%	12%	Stage 1
15.5 - 21	34%	15%	Stage 2
21 - 26	41%	22%	Stage 2
26 - 38	50%	27%	Stage 3
38 - 48	60%	36%	Stage 3
48 - 114	72%	56%	Stage 4

Table 4.1 Mean decrease in a- and b-wave amplitude in various affected groups. ERG recordings were obtained from 97 Abyssinian cats with hereditary retinal degeneration over 7 year period. (Whiting, Madsen & Narfstrom, 2008)

In Figure 4.8, the age groups of diseased cats were plotted against the mean amplitude decrease in a-wave. The data were fitted with a polynomial function and logarithmic function.

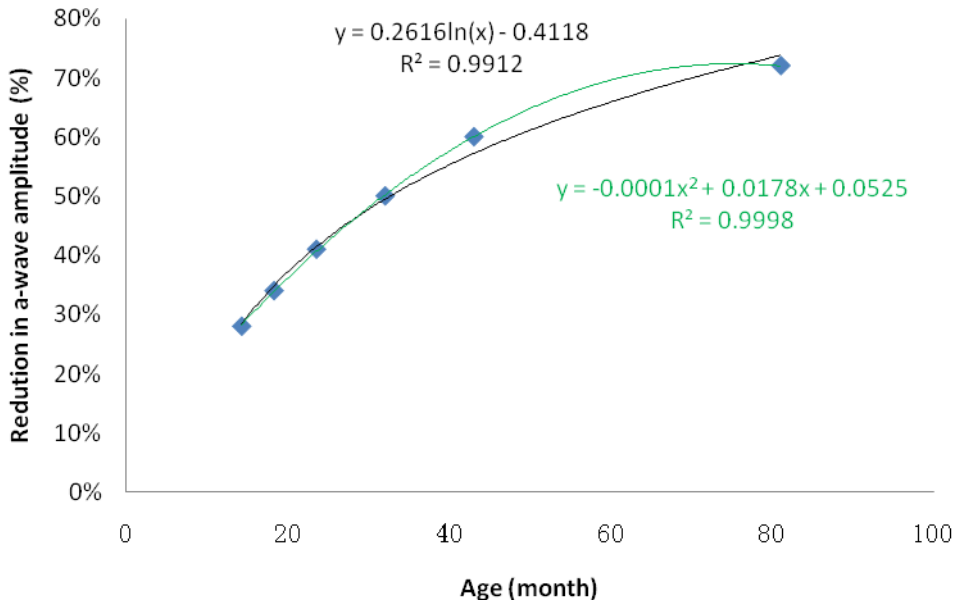

Figure 4.8 The mean amplitude decrease in a-wave versus different age groups of diseased cats, with respect to the normal group.

In Figure 4.9, results from Figures 4.7 and 4.8 were combined to find a relation between age and reduction in transport through the connecting cilium. With older age, the reduction in connecting cilium ionic transport becomes more severe. The trend can be approximated with a logarithmic function. This gives a way to estimate the reduction in CC transport as a function of age.

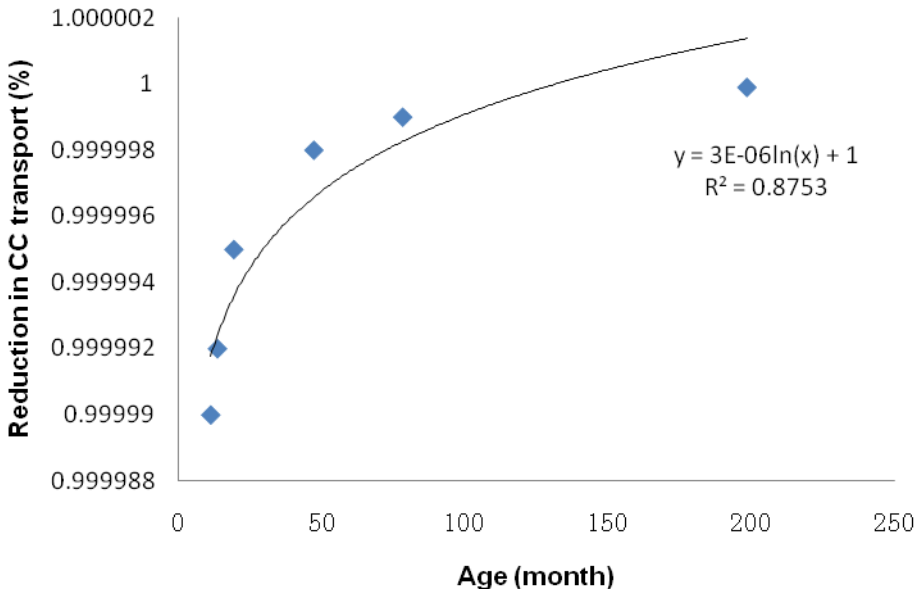

Figure 4.9 Reduction of ionic transport through connecting cilium (CC) versus age of diseased cats. The trend can be approximated by a logarithmic function, y=3e-6*ln(x)+1, with R^2=0.8753.

4.3 Receptor Response with Degeneration in K_x Channels

In this section, model simulations were performed for the conditons where ion transport through K_x channels were changed.

Figures 4.10 and 4.11 show the peak-point-values of the circulating current with respect to changes in K_x channel resistance ($R_{Kx)}$ and conductance (G_{Kx}), respectively. The total circulating current is reduced in a non-linear fashion (close to an exponential shape) with a decrease in K_x channel conductance.

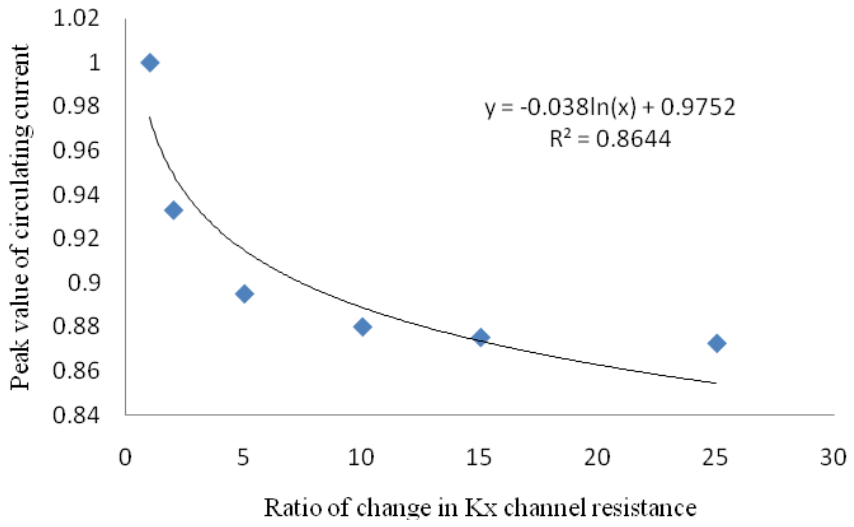

(A) Plain scale

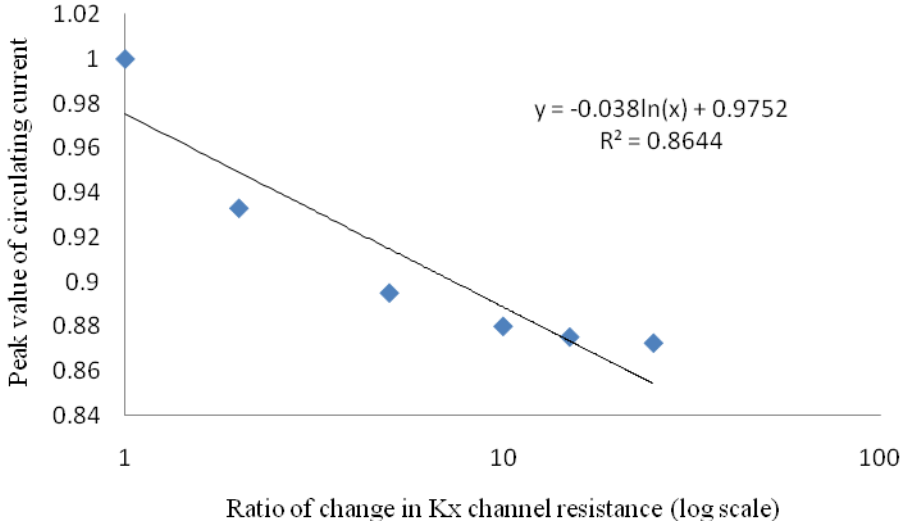

(B) Semi log scale

Figure 4.10 Changes in the peak-point value of circulating current with respect to changes in K_x channel resistance R_{Kx} in logarithmic scale.

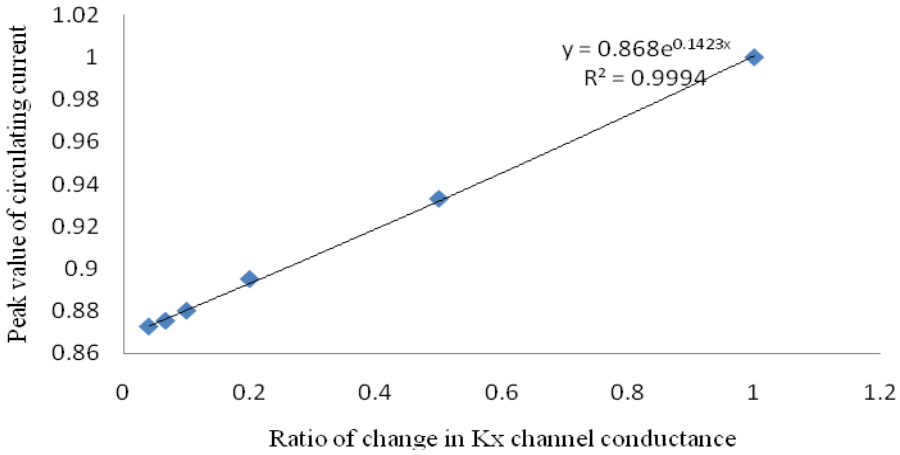

(A) Plain scale

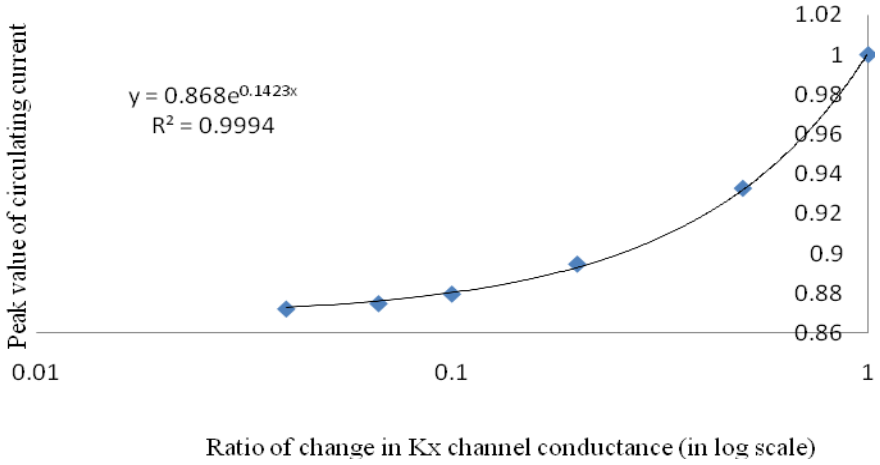

(B) Semi log scale

Figure 4.11 Changes in the peak-point value of circulating current with respect to changes in K_x channel conductance G_{Kx} in logarithmic scale.

With reduction in ion transport through K_x channels, ion concentrations and membrane potentials also vary. The amplitude of change observed is not only proportional to the reduction ratio in K_x channel conductance, but also influenced by accompanying changes in

ion transport through all other channel types and the connecting cilium, which was close to the actual situation. Figure 4.12 shows variation in membrane voltage and ionic concentrations of Na^+, K^+ and Ca^{2+}, with respect to changes in K_x channel resistance. With increased resistance, concentrations and membrane voltage levels increase non-linearly.

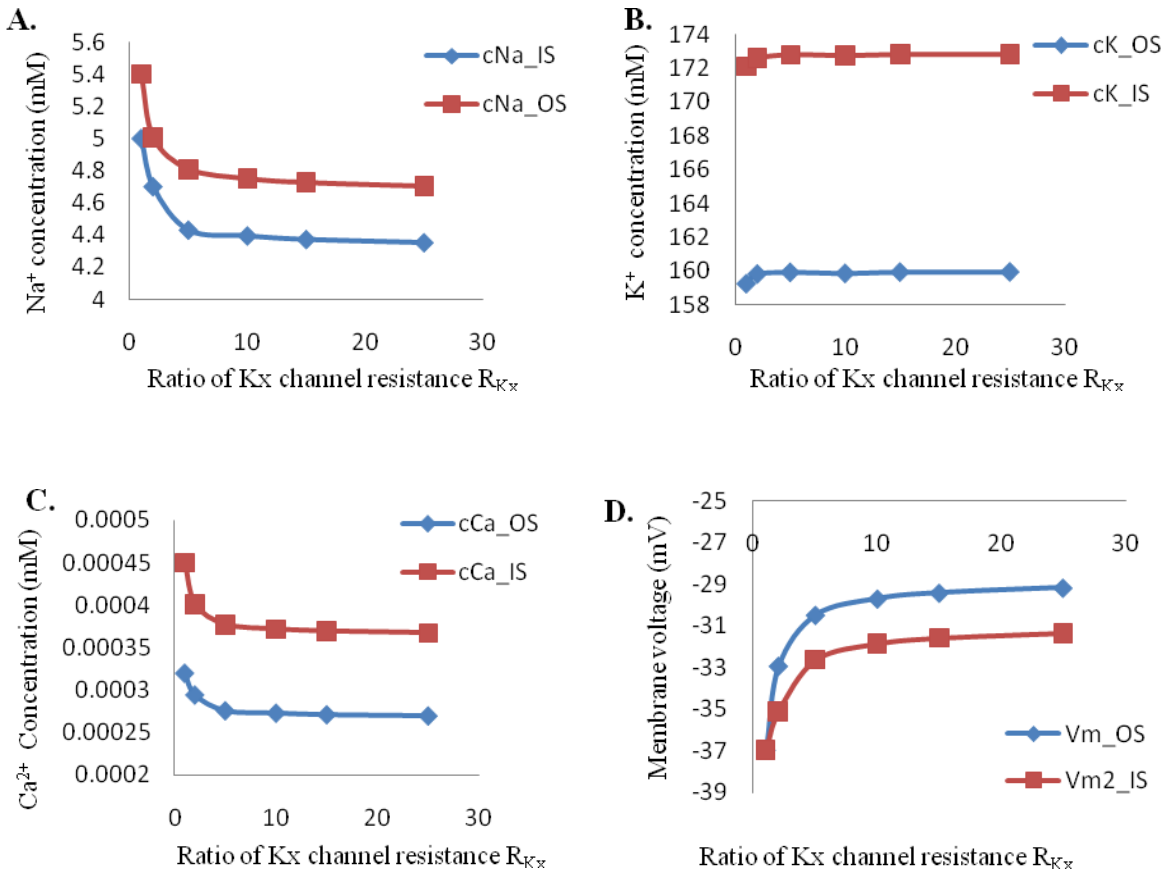

Figure 4.12. Changes in ion concentrations and membrane voltage (V_m) with respect to changes in K_x channel resistance. (A) Na^+ concentration v.s. K_x channel resistance; (B) K^+ concentration v.s. K_x channel resistance; (C) Ca^{2+} concentrations v.s. K_x channel resistance; (D) membrane voltage v.s. K_x channel resistance. cNa_IS, inner compartment Na^+ concentration; cNa_OS, outer segment Na^+ concentration; cK_IS, inner compartment K^+ concentration; cK_OS, outer segment K^+ concentration; cCa_IS, inner compartment Ca^{2+} concentration; cCa_OS, outer segment Ca^{2+} concentration; Vm_IS, inner compartment memebrane voltage; cNa_OS, outer segment memebrane voltage;

4.4 Discussion

From the model, we can analyze the major roles of different ion channels in the response process, the relationship between ion concentration changes and the measured response current. Moreover, it can also help to show the physiological processes associated with the channel activities. Analysis using this model could help to predict how the photoresponse would change given different stimuli or various disease stages of a photoreceptor cell, or reversely, help to determine the disease stage from recorded photoresponse or ERG waves.

One of the advantages offered by this model is that it needs only two types of input. Based on the input, all the ionic conductances (ion channels, ion exchangers and pumps) and other ion concentrations can then be estimated from the model. The inputs are (1) the dark circulating current, and (2) concentrations of ions or dark membrane potential in either the outer segment or the inner compartment.

ERG a-wave vs. receptor response of a single rod cell

By comparing the model simulation of bright-flash response with the experiment results, the model is proven to have a correct structure. The model can generate receptor responses of different amplitudes and shapes to varied flash intensities, and the simulated curves resemble experimental data in shape.

The data used to validate the model were ERG recordings that had a-, b- and c-waves, while the model generated only rod photoreceptor responses whose initial part is the a-waves.

Nontheless, in light of the changes in the peak amplitude of a-wave and the timing of b-wave initiation, the model still makes sense. Further improvement of the model can be made by including the b-wave initiation and experiments that provide only the receptor responses.

Some interesting observations

Although the outer segment and inner compartment are connected, the steady-state analysis shows that the ionic environments within are not the same for the two chambers. This includes the differences in ion concentrations, membrane voltages, and electric capacitance of the chambers that define the receptor response characteristics.

Comparison of ionic activities within the inner compartment and outer segment shows that the outer segment always exhibits greater shifts in response to changes applied to the photoreceptor, such as varied flash intensity and reduction of transport in the CC.

A number of questions arise. How might these differences contribute to the normal function of a photoreceptor cell? Would the receptor response be quite different if the ionic environments in the outer segment and inner compartment were made to be the same and still within normal physiological range? Would that eventually affect the normal function of the cell? Future work may need to consider these questions.

The resetting of the dark resting state (including dark circulating current and ion distributions) and peak receptor response as a result of abnormality in the connecting cilium transport showed some interesting results. When transport through the connecting cilium is

reduced, there are evident changes in the receptor response. The changes become significant and rapid when the CC conductance is reduced to a similar magnitude to that of ion channels in a rod cell membrane, whereas small reductions do not seem to induce much variation in the response. The latter is in agreement with the experimental observation that functional reduction of vision does not become evident until the disease has progressed to a relatively severe stage.

One thing worthy of investigating is the elevated Ca^{2+} concentration level in the outer segment, as a result of CC reduction. Given the roles of Ca^{2+} in many important cellular mechanisms, this change in Ca^{2+} concentration is likely to affect outer segment function.

What influence do changes in CC exert on a rod photoreceptor response?

Although the gene considered responsible for the disease is found to be localized to the rod connecting cilium, how exactly can it affect the area and thus, the whole mechanism, is still not clear.

First things to admit would be that multiple processes or mechanisms can be affected to make the disease progress, and among them one or some plays a bigger role.

If we assume dysfunction in CC to be one of the major factors, preliminary questions arise as: what processes would CC dysfunction influence? And can ion transport through CC change the photoreceptor response? If so, are the changes similar to that observed in diseased cats? Answer to the first question is complex and difficult to find out at this stage. For the last

two questions, results from previous sections provide some positive answers.

What we propose is that, by simulating and tracing the ionic activities, it would allow us to pin-point the biophysical processes that are most influenced by the disease. One of the strengths given by this approach is that the ionic activity is one that strings up the whole biophysical process within a photoreceptor; hence it can reflect the function of mechanisms underneath and provide information for diagnosis, even though it may not be the sub-process that is directly affected.

The cellular processes affected by the disease are likely to be linked together, and have causal effects on one another. The final outcome will then be an integration of all influences. When using the model to elucidate the processes that may participate in the progression of disease, this is a complexity. For this reason, we also present section 4.3 as an example on how interruption of a rod channel type (K_x channel) function may affect the photoreceptor response.

CHAPTER 5

CONCLUSIONS AND FUTURE WORK

5.1 Conclusions

In this research, a mathematical model was developed for the ionic activities that occur inside a rod photoreceptor. The model was applied to analyze the dark resting state of the rod photoreceptor cell, and to simulate the receptor response to light stimuli in normal and diseased rods. Different from other models that use empirical fittings, this model is based on a biophysical analysis.

Results from model validation, analysis of the dark resting state in different environments, and simulations lead to the following conclusions:

1. The model has a structure that can effectively describe the rod photoreceptor response to different stimuli and at varied photoreceptor disease stages.
2. The model can provide quantitative information of ionic activities, changes in ion concentration levels and membrane voltages in the inner compartment and outer segment.
3. The ionic environment is found to be different for the outer segment and the inner compartment.
4. During the receptor response, changes in the outer segment appear to be stronger and quicker than those of the inner and membrane voltage changes.

5. Model simulations showed that reduction in transport via the connecting cilium can reset the dark resting state and reduce the receptor response, which is in agreement with the ERG a-wave recordings of Abyssinian cats with inherited photoreceptor degeneration. Membrane voltage and Ca^{2+} concentrations are both higher in the outer segment when the connecting cilium is reduced.
6. While further work is needed, the model shows potential for analyzing and pin-pointing the processes involved in rod photoreceptor responses that might be affected and to assist further investigations.

5.2 Recommendations for Future Work

For the present model, the following future research efforts may be worth considering:

1. Include the phototransduction processes in the model so that the model can quantitatively account for the phototransduction reactions.

2. Further improve the model to include the b-wave.

3. Additional experiments to validate and improve the model. Experimental measurements of membrane voltage and ion concentrations, single-cell recordings, and effective chemical or genetic methods to isolate the a-waves are among the desirable experiments.

3. Modify the model so that it can better relate to the underlying biochemical and physiological processes and more effectively reveal the processes of disease.

APPENDIX

Computer program for model simulation:

```
#define MAXPTNUM 8001
#include <stdio.h>
#include <stdlib.h>
#include <math.h>

void SlopeCal(double c [],double Vm1,double Vm2, double R [], double slope [])
{
	double Vcyto1=19e-18;
	double Vcyto2=20e-18;
	double F=96320;
	double zqkt=37.38257;
	double Nae=145;
	double Ke=4;
	double Cae=1;
	int i;

	slope[0]=-zqkt*Vm1*Nae/R[0]+(Nae-c[0])/R[0]+5e-12*c[4]*c[2]/(320e-6*159.2328562146920)+zqkt*(Vm2-Vm1)*c[0]/R[8]+(c[1]-c[0])/R[8];//*c(2)/R(9)+(c(2)-c(1))/R(9);
	slope[0]=slope[0]/F/Vcyto1;

	slope[1]=-zqkt*Vm2*Nae/R[2]+(Nae-c[1])/R[2]-23e-12*c[1]/5.40218136376327-zqkt*(Vm2-Vm1)*c[0]/R[8]-(c[1]-c[0])/R[8];//*c(2)/R(9)-(c(2)-c(1))/R(9);
	slope[1]=slope[1]/F/Vcyto2;

	slope[2]=-1.25e-12*c[4]*c[2]/(320e-6*159.2328562146920)+zqkt*(Vm2-Vm1)*c[2]/R[9]+(c[3]-c[2])/R[9];//*c(4)/R(10)+(c(4)-c(3))/R(10);
	slope[2]=slope[2]/F/Vcyto1;

	slope[3]=-zqkt*Vm2*Ke*(1/R[3]+1/R[4]+1/R[5])+(Ke-c[3])*(1/R[3]+1/R[4]+1/R[5])+(15+1/3)*1e-12*c[1]/5.40218136376327-zqkt*(Vm2-Vm1)*c[2]/R[9]-(c[3]-c[2])/R[9];//*c(4)/R(10)-[c(4)-c(3)]/R(10);
	slope[3]=slope[3]/F/Vcyto2;

	slope[4]=-zqkt*Vm1*Cae*2/R[6]+(Cae-c[4])/R[6]-2.5e-12*c[4]*c[2]/(320e-6*159.2328562146920)+zqkt
```

```
*(Vm2-Vm1)*c[4]*2/R[1]+(c[5]-c[4])/R[1];//*c(6)*2/R(2)+[c(6)-c(5)]/R(2);
        slope[4]=slope[4]/F/Vcyto1/2;

        slope[5]=-zqkt*Vm2*Cae*2/R[7]+(Cae-c[5])/R[7]-zqkt*(Vm2-Vm1)*c[4]*2/R[1]-(c[5]-c[4])/R[1];//*c(6)
*2/R(2)-[c(6)-c(5)]/R(2);
        slope[5]=slope[5]/F/Vcyto2/2;

}

  main()
{

//Steady state calculation----------beginning
        static double x[15];
        double Nae,Ke,Cae,x2_6,x2_7,coeffx11,dt,start,t1,t2,t3,t4,totT,tcount,tau1,Vm1,Vm2;
        long PNum,filM,totdatap,RRatio,cGMPchannelratio;
        long i,cij,jj;
        long indexfilm,filMCount;
        double AcculWaveC;
        int iDebugCount;

        static double c[6][MAXPTNUM];
        static double IphrC[MAXPTNUM];
        static double IphrBattery[MAXPTNUM];
        static double WaveC[MAXPTNUM];
        static double WaveBattery[MAXPTNUM];
        static double vm1_plot[MAXPTNUM];
        static double vm2_plot[MAXPTNUM];
        static double tplot[MAXPTNUM];
        static double     R[10],R0[10];
        static double cnewlast[6];
        static double cpre[6];
        static double kn1[6],kn2[6],kn3[6],kn4[6],knTemp[6];

        double
        RcgNa,RthNa,RthK,RK,RKx,RKCa,RcgCa,RthCa,RCa,KK1,KK2,RhcnK,RhcnNa,RohcnK,RohcnNa;
        double curtime;
        double CloseRatio;
        double I_CNG,I_Kx_Ih;
```

```
double tempx1,tempx2,tempx3;
double pi=3.14159265358979;

FILE *fp;
if((fp=fopen("result.txt","w"))==NULL)
{
	printf("\nFaile to creat result.txt\n");
	fclose(fp);
	exit(0);
}

x[7]=-37e-3;
x[8]=-39e-3;
x[9]=5;
x[12]=172.1;
x[13]=320e-6;
x[14]=450e-6;
Nae=145;
Ke=4;
Cae=1;

x2_6=0.79/1.33;
x2_7=0.79/1.96;

printf("x[7]=%e\n",x[7]);

x[0]=37.38257*Nae*x[7]-145+x[9];//%%%
x[0]=-x[0]/18e-12;

printf("x(1)=%e\n",x[0]);

x[2]=37.38257*Ke*x[8]-4+x[12];
x[2]=x[2]/(14+1/12)*1e12;
printf("x(3)=%e\n",x[2]);

x[3]=2*37.38257*x[7]*Cae-1+x[13];
x[3]=-x[3]/2e-12;
printf("x(4)=%e\n",x[3]);
```

```
x[4]=2*37.38257*x[8]*Cae-1+x[14];
x[4]=-x[4]/0.5e-12;
printf("x(5)=%e\n",x[4]);

x[1]=-37.38257*x[14]*(x[8]-x[7])*2-x[14]+x[13];
x[1]=-x[1]/0.5e-12;
printf("x(2)=%e\n",x[1]);

x[5]=x[1]*x2_6;
x[6]=x[1]*x2_7;

printf("x(6)=%e\n",x[5]);
printf("x(7)=%e\n",x[6]);

coeffx11=37.38257*(x[8]-x[7])+1;
x[10]=x[9]-23e-12*x[5];
x[10]=x[10]/coeffx11;
printf("x(11)=%e\n",x[10]);

x[11]=-1.25e-12*x[6]+coeffx11*x[12];
printf("x(12)=%e\n",x[11]);

printf("x(12)=%e\n",x[11]);


dt=0.000000005;

start=0.02;
//  start=start*2;
//  start=start/20;
//  start=start*32;
//  start=start*2; start=start*2;
//  start=start*2;
start=start*2;

t1=0.0015; t2=0.0025; t3=0.012; t4=0.008;
t1=0.002; t2=0.00125; t3=0.009; t4=0.001;
t1=t1*2;t1=t1+t2;                    t4=t4*2;
t2=0;                                t4=t4*2;
```

```
                                        //t4=t4*2;
                                            //t4=t4*2; //%test 8 10000000Rthr
                                            //t4=t4*2; //%test 8 10000000Rthr
                                            //t4=t4*2; //%test 8 10000000Rthr
                                            //t4=t4*2; //%test 8 10000000Rthr

  //%% 01: Strong light stimulus -- As above %%%
  tau1=0.01;    //% Time constant(dark)=1ms

  //%% 02: Small stimulus -- t1 smaller & tau1 bigger %%%
  t1=t1/2; t1=t1/2;
  tau1=tau1*2; //////control stimulation 00
  cGMPchannelratio=1; //5; //40; ////////////////////////////////////////////////////////

  //tau1=tau1*2; //////smaller stimulation 01
  //tau1=tau1*32; //////smaller stimulation 02
  //tau1=tau1*32*32;
  //tau1=tau1*32*32;

  // %%% 03: Smaller stimulus -- t1 smaller(<02) & tau1 same(=02) %%%
  //
/////////// tau1=tau1*2;

  t1=t1*2; t2=t2*2; t3=t3*2; t4=t4*2;
  t1=t1*2; t2=t2*2; t3=t3*2; t4=t4*2;
  t1=t1*2; t2=t2*2; t3=t3*2; t4=t4*2;
  t1=t1*2; t2=t2*2; t3=t3*2; t4=t4*2;
  t1=t1*2; t2=t2*2; t3=t3*2; t4=t4*2;
  t1=t1*2; t2=t2*2; t3=t3*2; t4=t4*2;

  //t1=0; t2=0; t3=0; t4=0;
  totT=t1+t2+t3+t4+start;

  filM=1000000;
  //totdatap=(int)(PNum/filM);
  totdatap=(totT/filM/dt);

  c[0][0]=x[9];
  c[1][0]=x[10];
```

```
c[2][0]=x[11];
c[3][0]=x[12];
c[4][0]=x[13];
c[5][0]=x[14];

RcgNa=x[0];
RthNa=x[5];

RthK=x[6];
RK=x[2];
RKx=RK*(7+1/24);
RKCa=RK*(7+1/24)/(6+1/24);

RcgCa=x[3];
RthCa=x[1];
RCa=x[4];

KK1=2.29125; //2.0e-3;%2.29125;
KK2=2.29100; //1.6e-3;%2.1;

RhcnK=1e200; //7.4916e13;
RhcnNa=1e200; //2.4972e13;
RohcnK=7.4916e13; //7.4916e13;
RohcnNa=2.4972e13; //2.4972e13;

RRatio=1;
RthCa=RthCa/RRatio; RthNa=RthNa/RRatio; RthK=RthK/RRatio;
//RthCa=RthCa/0.0001; RthNa=RthNa/0.0001; RthK=RthK/0.0001;
// Change R here //

R[0]=RcgNa; R[1]=RthCa; R[2]=RhcnNa; R[3]=RKx; R[4]=RhcnK;
R[5]=RKCa; R[6]=RcgCa; R[7]=RCa; R[8]=RthNa; R[9]=RthK;

for (i=0;i<11;i++)
{
      R0[i]=R[i];
}
```

```
        vm1_plot[0]=x[7];//Vm1;
        vm2_plot[0]=x[8];//Vm2;
        printf("vm1_plot[0]=%e\n",vm1_plot[0]);
        printf("vm2_plot[0]=%e\n",vm2_plot[0]);

        Vm1=x[7];//Vm1;
        Vm2=x[8];//Vm2;

        for (i=0;i<6;i++)
        {
              cnewlast[i]=c[i][0];
        }

        AcculWaveC=0;

        filMCount=0;
        indexfilm=0;

    curtime=0;

iDebugCount=0;

////////////////////////////////////////////////////////////////////////////////
    for(tcount=dt;tcount<=totT;tcount+=dt)

    {
        //iDebugCount++;
        //if(iDebugCount==3*filM+1)
        //{
              //tcount=totT+10;
        //}

          for (cij=0;cij<6;cij++)
          {
                cpre[cij]=cnewlast[cij];
          }

        curtime=curtime+dt;
          CloseRatio=5;
```

```
        //if (curtime<=0.000000002 && curtime>=0.000000002)
        //{
        //      Vm1=Vm1;
        //}
//%-------------------------------------------------------------------%%

        if (curtime>start && curtime<=start+t1) //01-03:0.03      %% cGMP channel closing
        {
                //R[0]= R0[0]*exp((curtime-start)/tau1) ;
                //R[6]= R0[6]*exp((curtime-start)/tau1) ;
                R[0]= R0[0]*(1+cGMPchannelratio*(1-exp(-(curtime-start)/tau1))) ;
                R[6]= R0[6]*(1+cGMPchannelratio*(1-exp(-(curtime-start)/tau1))) ;
        }

        else if (curtime>=start+t1+dt && curtime<=start+t1+dt)
        {
                printf("R(1)=%e\n",R[0]);
                printf("Vm1=%e\n",Vm1);
        }

        if (Vm2>-72e-3 && Vm2<x[8]-1e-3 )//RKx
        {
                R[3]=1/(0.5*(1-cos(pi*(Vm2+72e-3)/(x[8]-1e-3+72e-3))))*R0[3];
        }

        else if (Vm2<=-72e-3)
        {
                R[3]=500*R0[3];//1e200;
        }
        else if (Vm2>=x[8]-1e-3)
        {
                R[3]=R0[3];
        }

        if (Vm2>-90e-3 && Vm2<x[8]-1e-3 )//Rhcn
        {
                R[2]=1/(0.5*(1+cos(pi*(Vm2+90e-3)/(x[8]-1e-3+90e-3))))*RohcnNa;
                R[4]=1/(0.5*(1+cos(pi*(Vm2+90e-3)/(x[8]-1e-3+90e-3))))*RohcnK;
```

```
  }
  else if (Vm2<=-90e-3)
  {
        R[2]=RohcnNa;
        R[4]=RohcnK;
  }
  else if (Vm2>=x[8]-1e-3)
  {
        R[2]=500*R0[2];//1e200;    %R0(3)
        R[4]=500*R0[4];//1e200;    %R0(5)
  }

  if (Vm2<=-46e-3) //RCa
  {
        R[7]=1e200;
  }
  else if (Vm2>-46e-3 && Vm2<x[8]-3e-3)
  {
        R[7]=1/(0.5*(1-cos(pi*(Vm2+46e-3)/(x[8]-3e-3+46e-3))))*R0[7];
  }
  else if (Vm2>=x[8]-3e-3)
  {
        R[7]=R0[7];
  }

if (cnewlast[5]<=80e-6) //RK(Ca)
{
        R[5]=500*R0[5];//1e200;
}
  else if (cnewlast[5]<200e-6)
  {
        R[5]=1/(0.5*(1-cos(pi*(cnewlast[5]-80e-6)/(200e-6-80e-6))))*R0[5];
  }
  else if (cnewlast[5]>=200e-6)
  {
        R[5]=R0[5];
  }

  if (curtime>start+t1+t2 && curtime<=start+t1+t2+t3 ) //%cGMP-gated take dt=t3 to recover
```

```
                {
                    // R[0]= R0[0]/(exp(-t1/tau1)+0.5*(1-cos(pi*(curtime-t1-t2-start)/t3))*(1-exp(-t1/tau1)));
                    // R[6]= R0[6]/(exp(-t1/tau1)+0.5*(1-cos(pi*(curtime-t1-t2-start)/t3))*(1-exp(-t1/tau1)));
                    R[0]=
R0[0]/(1/(1+cGMPchannelratio*(1-exp(-t1/tau1)))+0.5*(1-cos(pi*(curtime-t1-t2-start)/t3))*(1-1/(1+cGMPchan
nelratio*(1-exp(-t1/tau1)))));
                    R[6]=
R0[6]/(1/(1+cGMPchannelratio*(1-exp(-t1/tau1)))+0.5*(1-cos(pi*(curtime-t1-t2-start)/t3))*(1-1/(1+cGMPchan
nelratio*(1-exp(-t1/tau1)))));
                    //R[0]= R0[0]*(1+cGMPchannelratio*(1-exp(-t1/tau1))) ;
                    //R[6]= R0[6]*(1+cGMPchannelratio*(1-exp(-t1/tau1))) ;
                }
                else if (curtime>start+t1+t2+t3)
                {
                    R[0]=R0[0];
                    R[6]=R0[6];
                }

            // %%---------------------------- after a-wave ----------------------------%%
            //%-----------------------------------------------------------------%%
            Vm1=(cpre[0]+cpre[2]+cpre[4]*2-Nae-Ke-Cae*2-(x[9]+x[11]+x[13]*2-Nae-Ke-Cae*2))*KK1+x[7];

        Vm2=(cpre[1]+cpre[3]+cpre[5]*2-Nae-Ke-Cae*2-(x[10]+x[12]+x[14]*2-Nae-Ke-Cae*2))*KK2+x[8];
            SlopeCal(cpre,Vm1,Vm2,R,kn1);
            for (cij=0;cij<6;cij++)
            {
                knTemp[cij]=cpre[cij]+0.5*dt*kn1[cij];
            }
            SlopeCal(knTemp,Vm1,Vm2,R,kn2);
            for (cij=0;cij<6;cij++)
            {
                knTemp[cij]=cpre[cij]+0.5*dt*kn2[cij];
            }
            SlopeCal(knTemp,Vm1,Vm2,R,kn3);
            for (cij=0;cij<6;cij++)
            {
                knTemp[cij]=cpre[cij]+0.5*dt*kn3[cij];
            }
```

```
SlopeCal(knTemp,Vm1,Vm2,R,kn4);
for (cij=0;cij<6;cij++)
{
    cnewlast[cij]=cnewlast[cij]+dt/6*(kn1[cij]+2*kn2[cij]+2*kn3[cij]+kn4[cij]);
}
for (jj=0;jj<6;jj++)
{
    if (cnewlast[jj]<0)
    {
        cnewlast[jj]=1e-10;
    }
}


    I_CNG =  - Vm1*37.38257*Nae/R[0] + (Nae-cnewlast[0])/R[0] - Vm1*2*37.38257*Cae/R[6]
+ (Cae-cnewlast[4])/R[6] +1.25e-12 ;     //% outer segment total current, i.e. CNG + exchanger current
    I_Kx_Ih =  - Vm2*37.38257*Nae/R[2] - Vm2*37.38257*Ke*(1/R[3] + 1/R[4] + 1/R[5]) -
Vm2*2*37.38257*Cae/R[7] + (Nae-cnewlast[1])/R[2] + (Ke-cnewlast[3])*(1/R[3]+1/R[4]+1/R[5]) +
(Cae-cnewlast[5])/R[7] - 23e-12/3;

    AcculWaveC=AcculWaveC+(I_Kx_Ih + I_CNG)*dt;
    filMCount=filMCount+1;
    if(filMCount==filM)
    {
        indexfilm=indexfilm+1;
        printf("indexfilm=%d\n",indexfilm);
        filMCount=0;
    }

    if( filMCount==0 && indexfilm<MAXPTNUM)
   {
        vm1_plot[indexfilm]=Vm1;
        vm2_plot[indexfilm]=Vm2;
        c[0][indexfilm]=cnewlast[0]; //%% %% %%
        c[1][indexfilm]=cnewlast[1];// %% %% %%
        c[2][indexfilm]=cnewlast[2]; //%% %% %%
        c[3][indexfilm]=cnewlast[3]; //%% %% %%
        c[4][indexfilm]=cnewlast[4]; //%% %% %%
        c[5][indexfilm]=cnewlast[5]; //%% %% %%
```

```
                    IphrC[indexfilm] = I_Kx_Ih + I_CNG;
                    IphrBattery[indexfilm] = (I_CNG - I_Kx_Ih - 42.5e-12)/2 ;
                    WaveC[indexfilm]=AcculWaveC;
                    WaveBattery[indexfilm]=1e9*IphrBattery[indexfilm]*dt;

                    IphrC[indexfilm] = IphrC[indexfilm]*1000000000;
                    IphrBattery[indexfilm] = IphrBattery[indexfilm]*1000000000;
                    WaveC[indexfilm]=WaveC[indexfilm]*1000000000;
                    WaveBattery[indexfilm]=WaveBattery[indexfilm]*1000000000;
                    tplot[indexfilm]=curtime;
                }
        }

        for (i=0;i<indexfilm;i++)
        {
            if(i<MAXPTNUM)
            {

        fprintf(fp,"%6.10f    %6.10f %6.10f %6.10f    %6.10f %6.10f %6.10f %6.10f %6.10f    %6.10f %6
.10f %6.10f\n",
                    tplot[i],WaveBattery[i],IphrC[i],IphrBattery[i],WaveC[i],vm1_plot[i],vm2_plot[i],
                    c[0][i],c[1][i],c[2][i],c[3][i],c[4][i],c[5][i]);
        }
        }
        fclose(fp);
}
```

REFERENCES

Aho, A. C., K. Donner, et al. (1993). "Visual performance of the toad (Bufo bufo) at low light levels: retinal ganglion cell responses and prey-catching accuracy." J Comp Physiol A **172**(6): 671-682.

Aiba, H., S. Fujimoto, et al. (1982). "Molecular cloning and nucleotide sequencing of the gene for E. coli cAMP receptor protein." Nucleic Acids Res **10**(4): 1345-1361.

Allen, R. R. (1978). "Bond graph models for plant biosystems." Comput Programs Biomed **8**(3-4): 149-164.

Attwell, D., S. Borges, et al. (1987). "Signal clipping by the rod output synapse." Nature **328**(6130): 522-524.

Badano, J. L., N. Mitsuma, et al. (2006). "The ciliopathies: an emerging class of human genetic disorders." Annu Rev Genomics Hum Genet **7**: 125-148.

Bader, C. R., D. Bertrand, et al. (1982). "Voltage-activated and calcium-activated currents studied in solitary rod inner segments from the salamander retina." J Physiol **331**: 253-284.

Bader, C. R., P. R. Macleish, et al. (1979). "A voltage-clamp study of the light response in solitary rods of the tiger salamander." J Physiol **296**: 1-26.

Barnes, S. (1994). "After transduction: response shaping and control of transmission by ion channels of the photoreceptor inner segments." Neuroscience **58**(3): 447-459.

Barnes, S. and B. Hille (1989). "Ionic channels of the inner segment of tiger salamander cone photoreceptors." J Gen Physiol **94**(4): 719-743.

Baylor, D. A. and T. D. Lamb (1982). "Local effects of bleaching in retinal rods of the toad." J Physiol **328**: 49-71.

Baylor, D. A., G. Matthews, et al. (1984). "Location and function of voltage-sensitive conductances in retinal rods of the salamander, Ambystoma tigrinum." J Physiol **354**: 203-223.

Baylor, D. A., B. J. Nunn, et al. (1984). "The photocurrent, noise and spectral sensitivity of rods of the monkey Macaca fascicularis." J Physiol **357**: 575-607.

Beech, D. J. and S. Barnes (1989). "Characterization of a voltage-gated K+ channel that accelerates the rod response to dim light." Neuron **3**(5): 573-581.

Buck, L. and R. Axel (1991). "A novel multigene family may encode odorant receptors: a molecular basis for odor recognition." Cell **65**(1): 175-187.

Cajal, S. R. (1972). "The structure of retina." Thomas, Springfield **I1**.

Chen, J., C. L. Makino, et al. (1995). "Mechanisms of rhodopsin inactivation in vivo as revealed by a COOH-terminal truncation mutant." Science **267**(5196): 374-377.

Cobbs, W. H. and E. N. Pugh, Jr. (1987). "Kinetics and components of the flash photocurrent

of isolated retinal rods of the larval salamander, Ambystoma tigrinum." J Physiol **394**: 529-572.

Ehinger, B., K. Narfstrom, et al. (1991). "Photoreceptor degeneration and loss of immunoreactive GABA in the Abyssinian cat retina." Exp Eye Res **52**(1): 17-25.

Einthoven, W. and W. A. Jolly (1908). "The Form and Magnitude of the Electrical Response of the Eye to Stimulation by Light at Various Intensities
" Quaterly Journal of Experimental Physiology
1: 373-416.
.

Enoch, J. M. and F. L. Tobey (1981). "Vertebrate Photoreceptor Optics." Springer, Berlin.

Fain, G. L., F. N. Quandt, et al. (1978). "Contribution of a caesium-sensitive conductance increase to the rod photoresponse." Nature **272**(5652): 466-469.

Finn, J. T., M. E. Grunwald, et al. (1996). "Cyclic nucleotide-gated ion channels: an extended family with diverse functions." Annu Rev Physiol **58**: 395-426.

Granit, R. (1933). "The components of the retinal action potential in mammals and their relation to the discharge in the optic nerve." J Physiol **77**(3): 207-239.

Grell, J., J. Bernstein, et al. (1999). "Graph-set analysis of hydrogen-bond patterns: some mathematical concepts." Acta Crystallogr B **55**(Pt 6): 1030-1043.

Hamm, H. E. (1998). "The many faces of G protein signaling." J Biol Chem **273**(2): 669-672.

Harosi, F. I. and F. E. Malerba (1975). "Plane-polarized light in microspectrophotometry." Vision Res **15**(3): 379-388.

Hestrin, S. (1987). "The properties and function of inward rectification in rod photoreceptors of the tiger salamander." J Physiol **390**: 319-333.

Holmgren, F. (1870). "Om Retinastromme." Ups Lakareforenings Forh **6**: 419-455

Hood, D. C. and D. G. Birch (1990). "The A-wave of the human electroretinogram and rod receptor function." Invest Ophthalmol Vis Sci **31**(10): 2070-2081.

Iiri, T., Z. Farfel, et al. (1998). "G-protein diseases furnish a model for the turn-on switch." Nature **394**(6688): 35-38.

Imai, Y. (1996). "Network thermodynamics: analysis and synthesis of membrane transport system." Jpn J Physiol **46**(3): 187-199.

Jeong, M. B., K. Narfstrom, et al. (2009). "Comparison of the effects of three different combinations of general anesthetics on the electroretinogram of dogs." Doc Ophthalmol **119**(2): 79-88.

Kang Derwent, J. J., L. Padnick-Silver, et al. (2006). "The electroretinogram components in Abyssinian cats with hereditary retinal degeneration." Invest Ophthalmol Vis Sci **47**(8): 3673-3682.

Katz, M. L., K. Narfstrom, et al. (2005). "Assessment of retinal function and characterization of lysosomal storage body accumulation in the retinas and brains of Tibetan Terriers

with ceroid-lipofuscinosis." Am J Vet Res **66**(1): 67-76.
Kim, T. S., D. M. Reid, et al. (1998). "Structure-function relationships and localization of the Na/Ca-K exchanger in rod photoreceptors." J Biol Chem **273**(26): 16561-16567.
Kraft, T. W., D. M. Schneeweis, et al. (1993). "Visual transduction in human rod photoreceptors." J Physiol **464**: 747-765.
Lagnado, L. and P. A. McNaughton (1990). "Electrogenic properties of the Na:Ca exchange." J Membr Biol **113**(3): 177-191.
Lamb, T. D. and E. N. Pugh, Jr. (1992). "A quantitative account of the activation steps involved in phototransduction in amphibian photoreceptors." J Physiol **449**: 719-758.
Lo, C. H., Y. K. Wong, et al. (2004). "Model-based fault diagnosis in continuous dynamic systems." ISA Trans **43**(3): 459-475.
Ludwig, J., T. Margalit, et al. (1990). "Primary structure of cAMP-gated channel from bovine olfactory epithelium." FEBS Lett **270**(1-2): 24-29.
Maricq, A. V. and J. I. Korenbrot (1988). "Calcium and calcium-dependent chloride currents generate action potentials in solitary cone photoreceptors." Neuron **1**(6): 503-515.
Maricq, A. V. and J. I. Korenbrot (1990). "Inward rectification in the inner segment of single retinal cone photoreceptors." J Neurophysiol **64**(6): 1917-1928.
Matthews, H. R., G. L. Fain, et al. (1990). "Light adaptation in cone photoreceptors of the salamander: a role for cytoplasmic calcium." J Physiol **420**: 447-469.
Menotti-Raymond, M., V. A. David, et al. (2007). "Mutation in CEP290 discovered for cat model of human retinal degeneration." J Hered **98**(3): 211-220.
Miller, J. L. and J. I. Korenbrot (1994). "Differences in calcium homeostasis between retinal rod and cone photoreceptors revealed by the effects of voltage on the cGMP-gated conductance in intact cells." J Gen Physiol **104**(5): 909-940.
Mixon, M. B., E. Lee, et al. (1995). "Tertiary and quaternary structural changes in Gi alpha 1 induced by GTP hydrolysis." Science **270**(5238): 954-960.
Molday, R. S. and U. B. Kaupp (2000). Handbook of Biological Physics **3**(eds D.G. Stavenga, W.J. DeGrip and E.N. Pugh Jr.): 143-181.
Molday, R. S. and L. L. Molday (1998). "Molecular properties of the cGMP-gated channel of rod photoreceptors." Vision Res **38**(10): 1315-1323.
Mombaerts, P. (1999). "Molecular biology of odorant receptors in vertebrates." Annu Rev Neurosci **22**: 487-509.
Nakatani, K. and K. W. Yau (1988). "Calcium and magnesium fluxes across the plasma membrane of the toad rod outer segment." J Physiol **395**: 695-729.
Narfstrom, K. (1983). "Hereditary progressive retinal atrophy in the Abyssinian cat." J Hered **74**(4): 273-276.
Narfstrom, K. (1985). "Progressive retinal atrophy in the Abyssinian cat. Clinical characteristics." Invest Ophthalmol Vis Sci **26**(2): 193-200.
Narfstrom, K. (1985). Retinal degeneration in a strain of Abyssinian cats: a hereditary, clinical,

electrophysiological and morphological study [medical dissertation]. Linkoping, Sweden, Linkoping University**:** 91 p.

Narfstrom, K. and B. Ekesten (1998). "Electroretinographic evaluation of Papillons with and without hereditary retinal degeneration." Am J Vet Res **59**(2): 221-226.

Narfstrom, L. K. and S. E. Nilsson (1983). "Progressive retinal atrophy in the Abyssinian cat: an update." Vet Rec **112**(22): 525-526.

Nikonov, S., N. Engheta, et al. (1998). "Kinetics of recovery of the dark-adapted salamander rod photoresponse." J Gen Physiol **111**(1): 7-37.

Pazour, G. J., S. A. Baker, et al. (2002). "The intraflagellar transport protein, IFT88, is essential for vertebrate photoreceptor assembly and maintenance." J Cell Biol **157**(1): 103-113.

Pazour, G. J. and J. L. Rosenbaum (2002). "Intraflagellar transport and cilia-dependent diseases." Trends Cell Biol **12**(12): 551-555.

Perlman, I. (2005). http://webvision.med.utah.edu/ERG.html#Historical%20view.

Piper, H. (1911). "Ueber die Netzhautströme." Arch Anat Physiol Leipzig: 85-132.

Pugh, E. N. and T. D. Lamb (2000). "Phototransduction in Vertebrate Rods and Cones: Molecular Mechanisms of Amplification, Recovery and Light Adaptation." Molecular Mechanisms in Visual Transduction **ed. Stavenga, W.J., W.J.de Grip & E.N. Pugh, Jr., pp.183-255. Amsterdam; New York; Elsevier**: 183-225.

Schneeweis, D. M. and J. L. Schnapf (1995). "Photovoltage of rods and cones in the macaque retina." Science **268**(5213): 1053-1056.

Schnetkamp, P. P. (1989). "Na-Ca or Na-Ca-K exchange in rod photoreceptors." Prog Biophys Mol Biol **54**(1): 1-29.

Schnetkamp, P. P. (1995). "Calcium homeostasis in vertebrate retinal rod outer segments." Cell Calcium **18**(4): 322-330.

Smith, N. P. and T. D. Lamb (1997). "The a-wave of the human electroretinogram recorded with a minimally invasive technique." Vision Res **37**(21): 2943-2952.

Snodderly, D. M., J. D. Auran, et al. (1984). "The macular pigment. II. Spatial distribution in primate retinas." Invest Ophthalmol Vis Sci **25**(6): 674-685.

Snyder, A. W. and R. Menzel (1975). "Photoreceptor Optics." Springer, Berlin.

Sondek, J., A. Bohm, et al. (1996). "Crystal structure of a G-protein beta gamma dimer at 2.1A resolution." Nature **379**(6563): 369-374.

Sprang, S. R. (1997). "G protein mechanisms: insights from structural analysis." Annu Rev Biochem **66**: 639-678.

Takio, K., R. D. Wade, et al. (1984). "Guanosine cyclic 3',5'-phosphate dependent protein kinase, a chimeric protein homologous with two separate protein families." Biochemistry **23**(18): 4207-4218.

Titani, K., T. Sasagawa, et al. (1984). "Amino acid sequence of the regulatory subunit of bovine type I adenosine cyclic 3',5'-phosphate dependent protein kinase."

Biochemistry **23**(18): 4193-4199.

Torre, V., H. R. Matthews, et al. (1986). "Role of calcium in regulating the cyclic GMP cascade of phototransduction in retinal rods." Proc Natl Acad Sci U S A **83**(18): 7109-7113.

Vaegan and K. Narfstrom (2008). "Amax to scotopic Imax diagnoses feline hereditary rod cone degeneration more efficiently than any other combination of long protocol electroretinogram parameters." Doc Ophthalmol **117**(1): 1-12.

Wall, M. A., D. E. Coleman, et al. (1995). "The structure of the G protein heterotrimer Gi alpha 1 beta 1 gamma 2." Cell **83**(6): 1047-1058.

Wollmuth, L. P. (1995). "Multiple ion binding sites in Ih channels of rod photoreceptors from tiger salamanders." Pflugers Arch **430**(1): 34-43.

Wollmuth, L. P. and B. Hille (1992). "Ionic selectivity of Ih channels of rod photoreceptors in tiger salamanders." J Gen Physiol **100**(5): 749-765.

Xu, J., R. L. Dodd, et al. (1997). "Prolonged photoresponses in transgenic mouse rods lacking arrestin." Nature **389**(6650): 505-509.

Zufall, F. and T. Leinders-Zufall (1998). "Role of cyclic GMP in olfactory transduction and adaptation." Ann N Y Acad Sci **855**: 199-204.